iScience

CellPress

Article

Live-Cell Imaging and Functional Dissection of *Xist* RNA Reveal Mechanisms of X Chromosome Inactivation and Reactivation

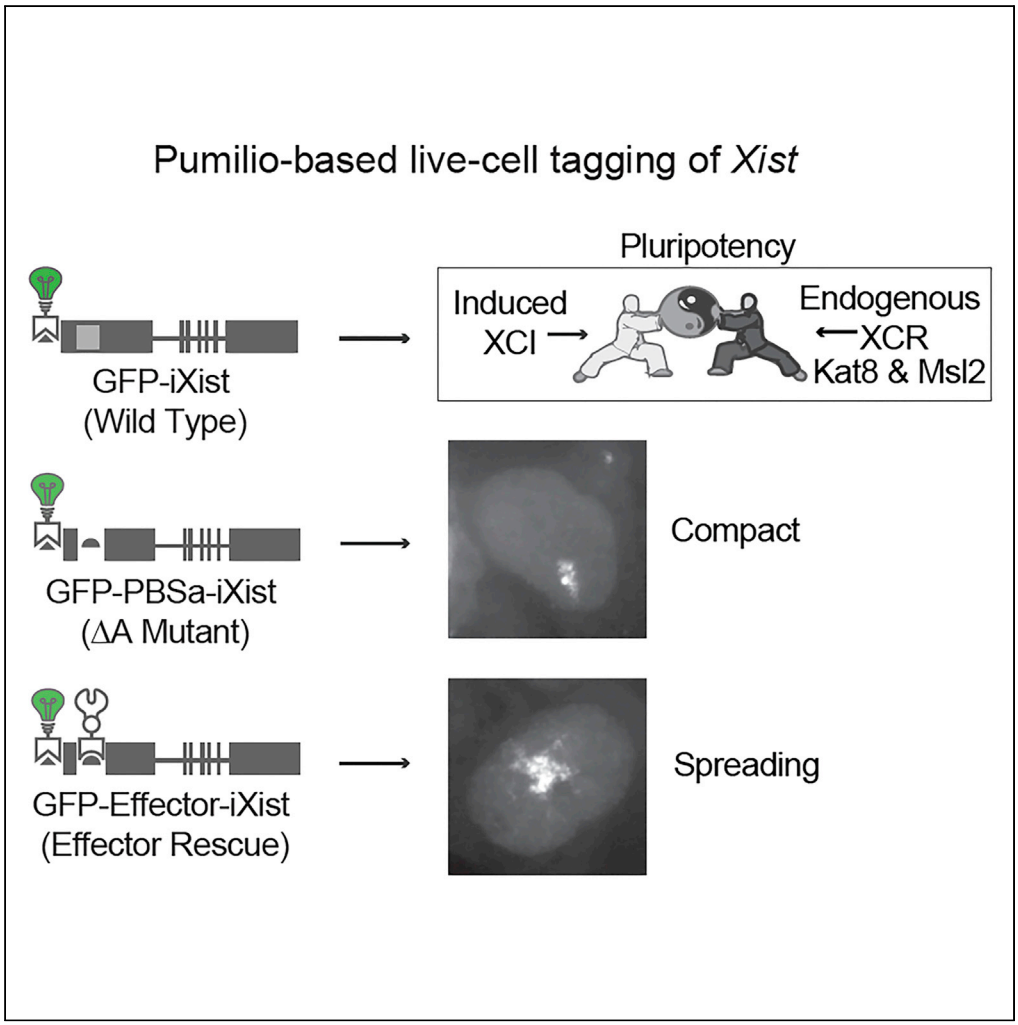

Norbert Ha, Lan-Tian Lai, Rosi Chelliah, ..., Sara Sandin, Lingyi Chen, Li-Feng Zhang

lingyichen@nankai.edu.cn (L.C.)
zhanglf@ntu.edu.sg (L.-F.Z.)

HIGHLIGHTS

A Pumilio-based system allows efficient double-tagging of *Xist* RNA in live cells

Induced XCI in undifferentiated ES cells reveals the roles of Kat8 and Msl2 in XCR

Live-cell imaging reveals the undersized "ΔA mutant" *Xist* signals

Tethering proteins onto "ΔA mutant" reveals their role in Xist-mediated silencing

Ha et al., iScience *8*, 1–14
October 26, 2018
https://doi.org/10.1016/j.isci.2018.09.007

iScience

CellPress

Article

Live-Cell Imaging and Functional Dissection of *Xist* RNA Reveal Mechanisms of X Chromosome Inactivation and Reactivation

Norbert Ha,[1] Lan-Tian Lai,[1] Rosi Chelliah,[1] Yashu Zhen,[1] Seet Pei Yi Vanessa,[1] Soak-Kuan Lai,[1] Hoi-Yeung Li,[1] Alexander Ludwig,[1] Sara Sandin,[1] Lingyi Chen,[2,*] and Li-Feng Zhang[1,3,4,*]

SUMMARY

We double-tagged *Xist* (inactivated X chromosome-specific transcript), a prototype long non-coding RNA pivotal for X chromosome inactivation (XCI), using the programmable RNA sequence binding domain of Pumilio protein, one tag for live-cell imaging and the other replacing A-repeat (a critical domain of *Xist*) to generate "ΔA mutant" and to tether effector proteins for dissecting *Xist* functionality. Based on the observation in live cells that the induced XCI in undifferentiated embryonic stem (ES) cells is counteracted by the intrinsic X chromosome reactivation (XCR), we identified Kat8 and Msl2, homologs of *Drosophila* dosage compensation proteins, as players involved in mammalian XCR. Furthermore, live-cell imaging revealed the obviously undersized ΔA *Xist* cloud signals, clarifying an issue regarding the previous RNA fluorescence *in situ* hybridization results. Tethering candidate proteins onto the ΔA mutant reveals the significant roles of Ythdc1, Ezh2, and SPOC (Spen) in *Xist*-mediated gene silencing and the significant role of Ezh2 in *Xist* RNA spreading.

INTRODUCTION

In mammalian female somatic cells, one of the two X chromosomes is silenced to compensate the X-linked gene dosage between males and females. This phenomenon is known as X chromosome inactivation (XCI) (Payer and Lee, 2008). Inactivated X chromosome-specific transcript (*Xist*) plays an essential role in XCI (Payer and Lee, 2008). Upon the initiation of XCI, *Xist* transcription is up-regulated from the future inactive X chromosome (Xi), and the RNA transcripts spread out to paint the entire chromosome territory to establish chromosome-wide gene silencing. Coating of the Xi by *Xist* transcripts produces an interesting *Xist* "cloud" signal in RNA fluorescence *in situ* hybridization (FISH) (Clemson et al., 1996). To date, labeling of *Xist* RNA in the cellular context is nearly exclusively achieved by RNA FISH. Visualizing the spatial distribution and dynamics of *Xist* RNA in live cells may provide important insights into the functional mechanism of *Xist*.

However, although various approaches have been proposed and developed (Urbanek et al., 2014), live-cell imaging of RNA remains technically challenging. A previous study reported that based on the interaction between an RNA motif (MS2 motif) from the MS2 phage and the MS2 RNA-binding protein (MCP), *Xist* RNA fused to a tandem array of MS2 motifs can be visualized by GFP-tagged MCP (MCP-GFP) (Ng et al., 2011). An inducible *Xist* cDNA transgene fused with 24 MS2 motifs at its 3′ end was constructed, and a transgenic cell line carrying 7 copies of the *Xist* cDNA transgene on chromosome 7 was established for live-cell imaging. Possibly due to technical limitations, the report did not provide any time-lapse video file to illustrate the RNA's behavior in live cells.

RESULTS

The Experimental System

In this study, we took advantage of programmable sequence-specific RNA binding by the Pumilio homology domain (PUF) to visualize *Xist* RNA in live cells (Wang et al., 2002; Cheong and Hall, 2006). A total of 25 copies of PUF binding sites (PBSb) (Cheng et al., 2016) were fused to the 5′ end of a full-length *Xist* transgene. An inducible *Xist* cell line was then generated from Ainv15 cells (Kyba et al., 2002), a male mouse embryonic stem (ES) cell line carrying an engineered cassette upstream of the X-linked *Hprt* gene (Figure 1A). Through Cre-mediated gene targeting, the transgene was inserted downstream of the tetracycline response element (TRE) of Ainv15 cells, restoring neomycin resistance (Figure 1A). Moreover, a red

[1]School of Biological Sciences, Nanyang Technological University, 60 Nanyang Drive, Singapore 637551, Singapore

[2]State Key Laboratory of Medicinal Chemical Biology, Key Laboratory of Bioactive Materials, Ministry of Education, Tianjin Key Laboratory of Protein Sciences and College of Life Sciences, Nankai University, Tianjin 300071, China

[3]Present address: Beijing Leadman Biochemistry Co., Ltd., No.5 Xinghai Road, BDA, Beijing, China

[4]Lead Contact

*Correspondence: lingyichen@nankai.edu.cn (L.C.), zhanglf@ntu.edu.sg (L.-F.Z.)

https://doi.org/10.1016/j.isci.2018.09.007

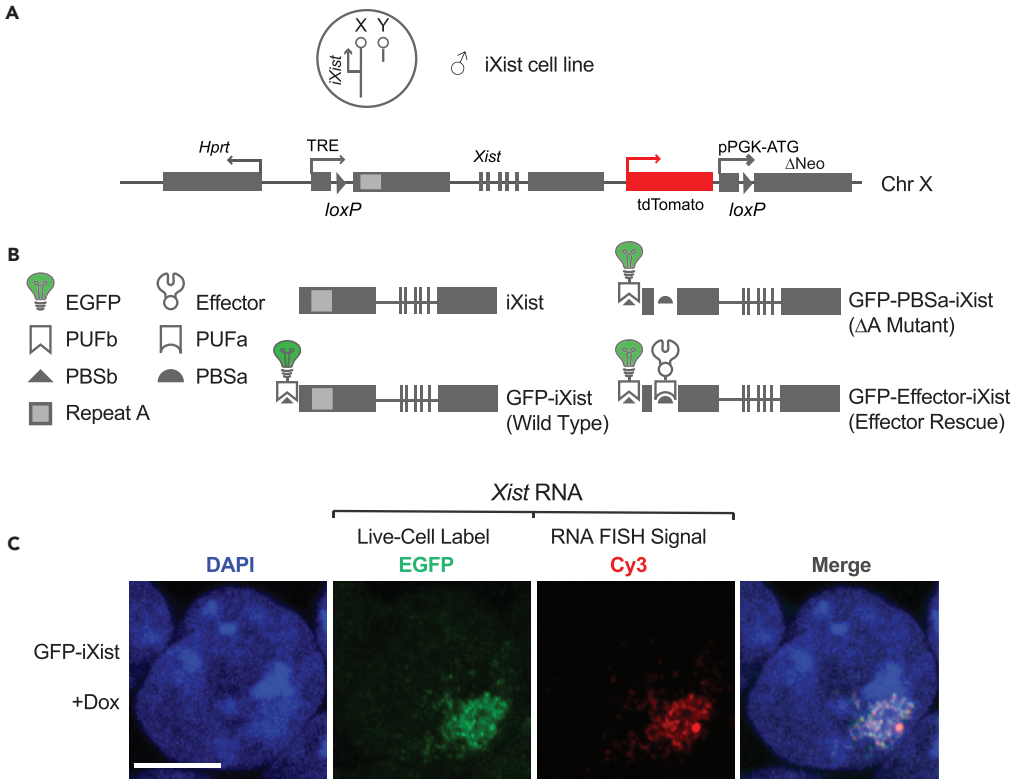

Figure 1. The Experimental System and the Inducible *Xist* Cell Lines

(A) Schemes of the iXist cell line and the inducible *Xist* allele. TRE, tetracycline response element; ΔNeo, the coding region of neomycin resistance gene without the start codon; pPGK-ATG: PGK promoter and a start codon.

(B) Diagrams of the live-cell imaging system and the different engineered inducible *Xist* alleles used in this study. PUF, Pumilio homology domain; PBS: PUF binding site.

(C) RNA FISH to validate live-cell labeling of *Xist*. The RNA FISH probe was Cy3-labeled (red). DNA was counterstained with DAPI (blue). The cell was imaged in high resolution by Airyscan Super-resolution Confocal Microscope (Carl Zeiss). The images shown are from a single Z-section. Note: although the emission spectrums of Cy3 and tdTomato are overlapping, the *Xist* RNA FISH signals were clearly detected. This is possibly due to the RNA FISH signal intensity and/or *Xist*-mediated gene silencing on the tdTomato reporter. Scale bar: 5 μm.

See also Figure S1.

fluorescent protein (tdTomato) was included as a reporter gene (Figure 1A). The resulting cell line is a male mouse ES cell line carrying an inducible, single-copy and full-length *Xist* transgene on its X chromosome (Figure 1A). Both neomycin resistance and tdTomato were used as reporters to assess the functionality of the inducible *Xist* transgene. Ectopic expression of PUFb-GFP fusion protein resulted in a cell line (GFP-iXist) that permits the spatiotemporal analysis of *Xist* RNA distribution and dynamics in live cells (Figure 1B).

To take advantage of the Pumilio system, which provides multiple PUFs and PBSs, we engineered an inducible *Xist* ES cell line in which the A-repeat of *Xist* was replaced by 10 copies of PBSa (Cheng et al., 2016) (GFP-PBSa-iXist) (Figure 1B). A-repeat is a conserved region of *Xist*, which is functionally important for *Xist*-mediated gene silencing (Wutz et al., 2002). GFP-PBSa-iXist can be regarded as a "ΔA mutant" of the inducible *Xist* transgene. Currently, a growing list of proteins are identified as proteins involved in XCI, including enhancer of zeste homolog 2 (Ezh2), a critical member of the polycomb repressive complex 2 (PRC2) (Plath et al., 2003; Cao et al., 2002); Spen (split end), a transcription repressor (McHugh et al., 2015, Chu et al., 2015, Minajigi et al., 2015, Monfort et al., 2015, Moindrot et al., 2015); and YTH domain-containing 1 (Ythdc1), a nuclear protein that recognizes N6-methyladenosine (m6A), binds directly to the A-repeat region, and plays a role in XCI (Patil et al., 2016). These proteins can be fused to PUFa, which helps to artificially tether individual candidate proteins back onto the ΔA mutant *Xist* transcripts as "effector" proteins (Figure 1B). This experimental system helps to further dissect the functionality of *Xist*

and its binding proteins. Ectopic expression of PUFa-effector fusion proteins resulted in additional transgenic cell lines (Figure 1B).

We validated the live-cell labeling of *Xist* in the established transgenic cell lines. With a 24-hr doxycycline (dox) treatment, GFP-labeled *Xist* clouds could be clearly detected in ~70%–90% of nuclei in all established cell lines (data not shown). *Xist* RNA FISH on fixed cells confirmed that the *Xist* signals labeled by GFP overlap with the RNA signal detected by the RNA FISH probe (Figure 1C). Since two PUFs are involved in this study and they are highly homologous to each other, we then tested the binding specificity of a PUF with its PBS. When PUFa-EGFP was expressed in a cell line carrying PBSb-*Xist* fusion, no *Xist* signals were detected after a 24-hr dox treatment (Figure S1A). This result confirms that there is no cross-reactivity between PUFa and PBSb. Furthermore, this result also helps to address the concern on the PBSa sites located within the endogenous sequence of *Xist*. We analyzed the sequence of the *Xist* gene body, including introns, and identified two PBSa sites and two antisense PBSa sites (Figure S1B). Meanwhile, no PBSb sites were identified (Figure S1B). It is a concern that the endogenous PBSa sites may interact with PUFa. It is also a probability in theory that the endogenous antisense PBSa sites may interact with the PBSa tag and in consequence affect the secondary structure of *Xist*. We performed multiple experiments to address these concerns. Here, the result that no *Xist* signals were observed in the induced cells overexpressing PUFa-EGFP (Figure S1A) shows that the endogenous PBSa sites did not result in "unspecific" signals in live-cell imaging.

The Difficulties of "Sunrise" in Undifferentiated ES Cells

With the established cell lines, we first examined the emergence and growth of *Xist* RNA signals upon dox treatment (the "sunrise" process). Live-cell imaging was performed 1 hr after dox treatment, which allowed us to monitor the sunrise process in most of the differentiating cells within the 2-hr time span of live-cell imaging. Interestingly, the sunrise behavior was markedly different between differentiating and undifferentiated ES cells. In differentiating cells, the *Xist* RNA signals emerged quickly (Figure 2A) and in a synchronized manner (Video S1). Most *Xist* RNA signals first appeared as small puncta that then gradually grew into ~2-μm-large *Xist* RNA clouds within 60–90 min (Figures 2B and S2). In undifferentiated cells, the onset of sunrise occurred later and was more heterogeneous (Figure 2A and Videos S2, S3, and S4). Some *Xist* RNA puncta gradually developed into clouds, very much like the *Xist* RNA signals in differentiating cells (we call this behavior "blossom"). However, a large fraction of *Xist* RNA puncta never showed significant growth within ~60 min (Figure 2C) (we call this behavior "star"). Even after a prolonged treatment with dox (2 hr) before live cell imaging, a significant fraction of undifferentiated cells did not develop *Xist* RNA clouds during the subsequent 2-hr time span of live-cell imaging (Videos S2, S3, and S4). In general, *Xist* RNA growth in undifferentiated cells was significantly slower than in differentiating cells (Figures 2D and 2E).

The "Tug of War" between the Induced XCI and the Intrinsic XCR

To further study the special sunrise behaviors, we examined the effects of induced *Xist* expression on X-linked genes. The induced *Xist* expression clearly repressed the transcription of X-linked genes in both undifferentiated (Figure S3) and differentiating cells (Figure 3A). However, *Xist*-mediated gene silencing is much weaker or inefficient in undifferentiated cells (Figure 3A). In the 6 X-linked genes tested, the induced *Xist* expression levels are comparable between undifferentiated and differentiating cells. *Hprt* showed a slightly higher expression level in differentiating cells than in undifferentiated cells, which can be explained by the close head-to-head orientation of the *Hprt* promoter and the *TRE* (Figure 1A). The strong transcriptional activity of *TRE* may cause hypermorphic expression of *Hprt*. The rest of the 4 X-linked genes tested all showed significantly lower expression levels in differentiating cells (Figure 3A). Therefore, the difficulties of sunrise in undifferentiated cells are associated with weaker *Xist*-mediated silencing.

The inducible *Xist* transgene is X-linked. Therefore, inducible *Xist* expression causes cell death and growth arrest due to *Xist*-mediated gene silencing along the single X chromosome in male cells. This "killing effect" of induced XCI can be used to assess the functionality of *Xist*-mediated gene silencing. Indeed, dox treatment showed a stronger killing effect in differentiating cells, which is consistent with the more efficient *Xist*-mediated gene silencing in differentiating cells (Figures 3B and 3C).

Moreover, it is known that the undifferentiated ES cells are maintained in culture in metastable pluripotent states with a heterogeneous population of Nanog-high and Nanog-low cells (Chambers et al., 2007). We observed that during the early hours of dox treatment, *Xist* clouds appear more frequently in

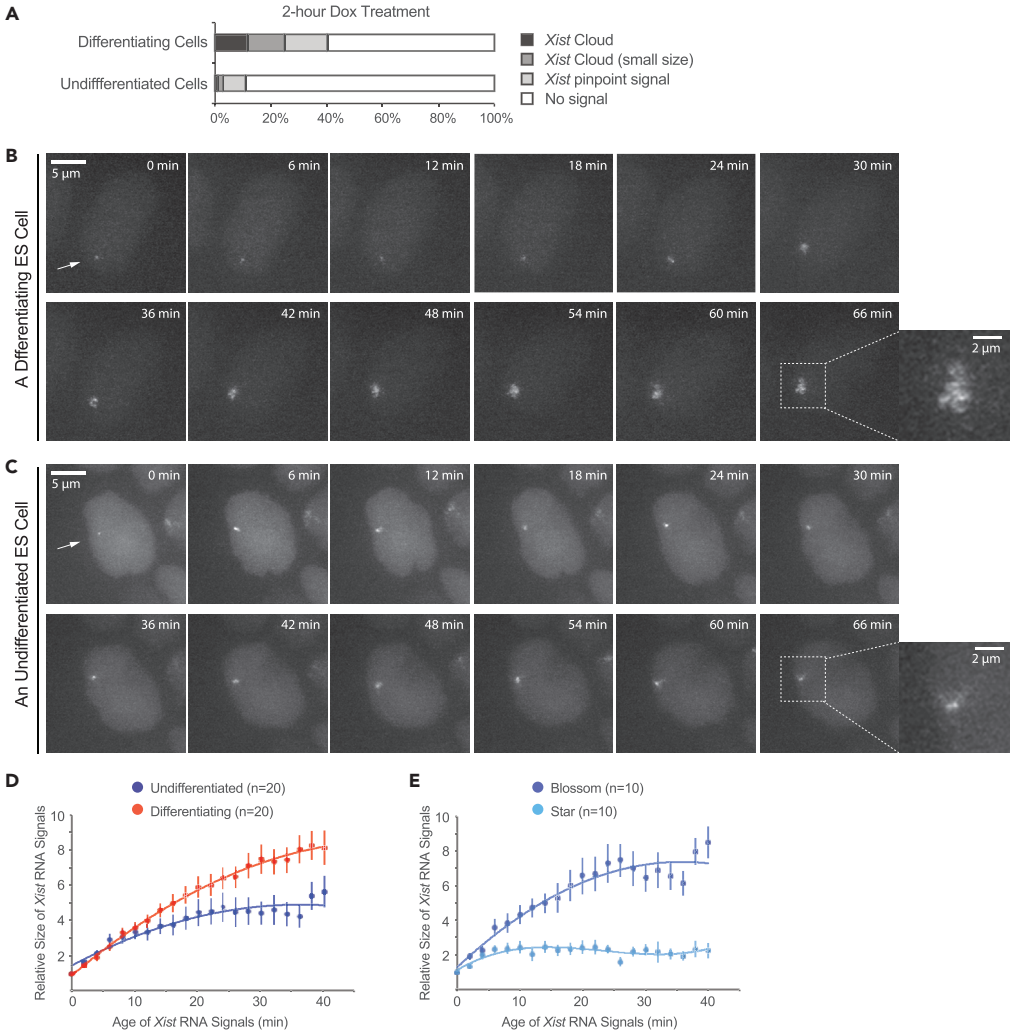

Figure 2. The Difficulties of "Sunrise" in Undifferentiated ES Cells

(A) *Xist* signals in live cells treated with dox for 2 hr.

(B and C) The emergence of *Xist* RNA signals in an (C) undifferentiated ES cell and a (B) differentiating ES cell. All the live-cell imaging, unless explicitly mentioned, was carried out in a 2-hr time span with a time interval of 2 min. For direct comparison between the two *Xist* signals, images are shown in a 66-min time span with a 6-min time interval. The time point when a signal was first detected is defined as time zero for the signal. Maximum intensity z projections are shown. Arrows point out the Xist clouds.

(D) The growth curves of *Xist* RNA signals. Measurements of *Xist* RNA signal size increment over time. The size (area) of a signal when it was first detected is defined as "size one" for the signal. *Xist* RNA signals were analyzed in 20 cells randomly selected from each sample. Data are shown as mean ± SEM with a trend line.

(E) The growth curves of "star" and "blossom," two behaviors of *Xist* RNA signal emergence in undifferentiated ES cells upon doxycycline treatment.

See also Figure S2 and Videos S2, S3, and S4.

Nanog-low cells (Figures 3D and S4). Taken together, these results argue for the biological significance underlying the difficulties of sunrise observed in undifferentiated cells.

It is well known that an undifferentiated ES cell is able to reprogram or dedifferentiate a somatic cell back to pluripotency, if the two cells are fused (Ohhata and Wutz, 2013). During this process, the Xi is also reactivated (Ohhata and Wutz, 2013). Therefore, a pluripotent mouse ES cell possesses a built-in capacity for X chromosome reactivation (XCR). We speculated that the induced XCI status in undifferentiated iXist cells is a balanced outcome of two counteracting forces, the induced XCI and the intrinsic XCR (Figure 3E). Thus,

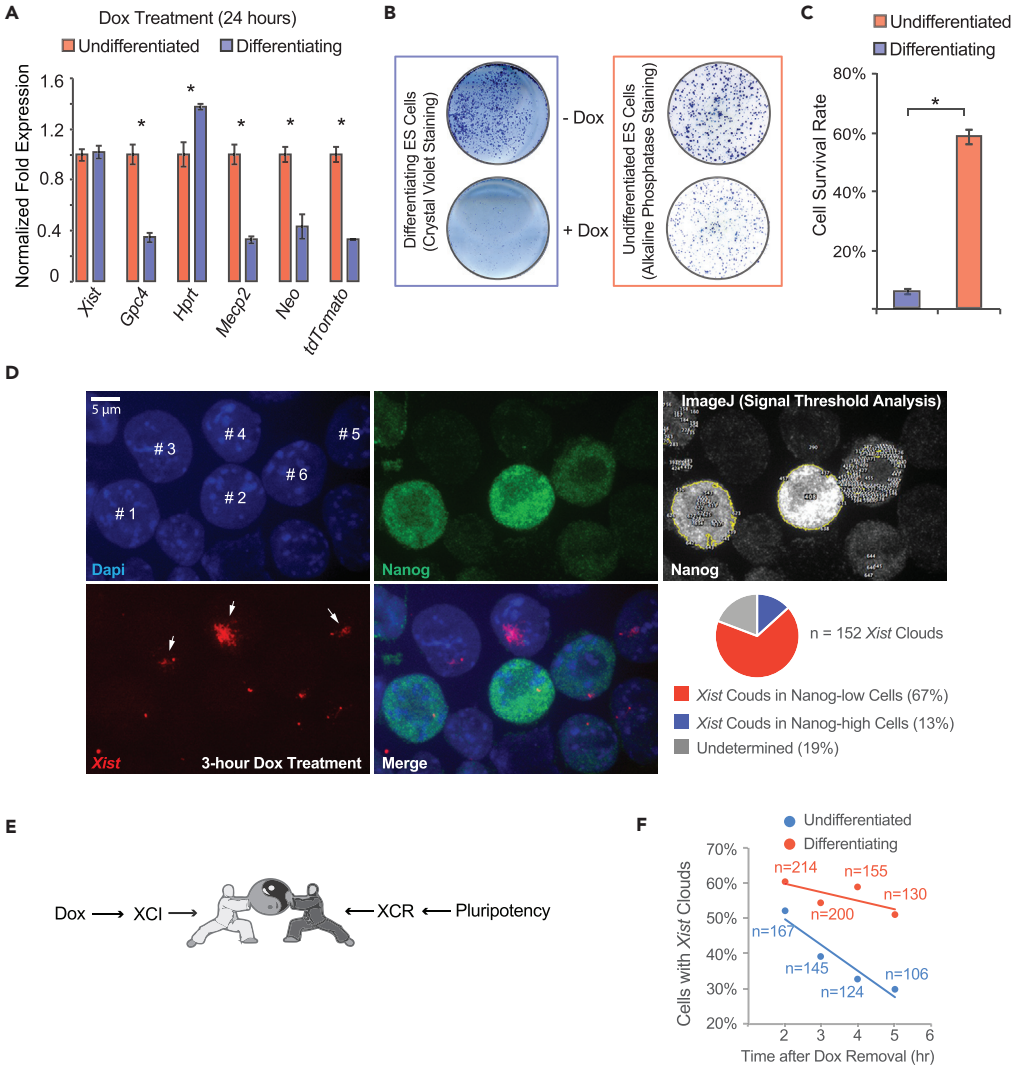

Figure 3. The "Tug of War" between Induced XCI and Intrinsic XCR

(A) Quantitative RT-PCR results to show the *Xist*-mediated silencing effect on X-linked genes between undifferentiated and differentiating cells. Doxycycline treatment was carried out for 24 hr. The results are shown in relative fold expression. Normalization was performed using *Actb* and *Gapdh*. The expression level of each gene in undifferentiated cells is set as 1. Error bars indicate SEM (n = 3). The statistical analysis used is Student's *t* test. p Value was calculated between the pair of datasets of each gene. *$p < 0.05$.

(B and C) (B) Doxycycline-induced cell death assay on iXist cells. Cells were cultured either as undifferentiated or as differentiating ES cells. Doxycycline treatment was carried out for 4 days. (C) Cell survival rate for differentiating cells was calculated by measuring the area stained by crystal violet staining. Cell survival rate for undifferentiated cells was calculated by alkaline phosphatase-stained colony counts. Data are shown as mean ± SEM of biological triplicate. The statistical analysis used is Student's *t* test. *$p < 0.05$.

(D) Immuno-RNA FISH to detect Nanog and *Xist* in undifferentiated iXist cells treated with dox for 3 hr. DNA was counterstained with DAPI (blue). Cells were cultured in the conventional Lif-containing ES culture medium without 2i. The nuclei in the image relevant for the discussion are labeled as #1–6. The RNA FISH probe was Cy3-labeled (red). White arrows indicate the three *Xist* cloud signals detected in nuclei #3–5. Nanog was detected by immunostaining (green). The Nanog-high and Nanog-low cells were identified by ImageJ with a selected signal intensity threshold. Nuclei #1 and #2 are Nanog-high, because the entire nucleus or a large part of it was recognized as a single "particle" (the yellow outline highlighting the perimeter) above the selected signal intensity threshold. Nucleus #6 could be grouped into either Nanog-high cells or undetermined cells depending on the subjectivity of the data analyzer. Nuclei #3–5 belong to Nanog-low cells.

(E) The counteracting forces of XCI and XCR determine the X inactivation status in undifferentiated iXist cells upon dox induction.

(F) The rate of *Xist* RNA signal disappearance upon doxycycline removal.

See also Figures S3–S5.

we examined the "sunset" process (disappearance of *Xist* signals upon dox removal), which reflects XCR. The results show that sunset proceeds at a faster rate in undifferentiated cells than in differentiating cells, indicating higher activity of XCR in undifferentiated cells (Figure 3F). Here, one concern is that the *Xist* clouds may dissipate more rapidly in fast dividing cells. To find out whether the faster sunset rate observed in undifferentiated cells is related to a faster cell division rate, we examined the cell division rates of the two samples during the 3-hr time window of the live-cell imaging experiment (Figure S5). Although undifferentiated ES cells divide faster than differentiating cells under normal tissue culture conditions, the cell growth rates may differ under the live-cell imaging experimental conditions. The cells (both undifferentiated and differentiating cells) were trypsinized shortly before the experiments. Cell colony formation and feeder cells were avoided for imaging purposes. Therefore, the trypsinized cells were directly attached to the fibronectin-coated glass surface of the MatTec dish in low cell density without feeder cells. The live-cell imaging experiments were then carried out within a 3-hr time window. Based on our measurements, the undifferentiated cells and the differentiating cells showed nearly identical cell division rates under these conditions (Figure S5). More importantly, limited amount of cell division was detected during the 3-hr time window of live-cell imaging. Taken together, the result of the sunset experiment rules out the technical concern that the difficulties of sunrise in undifferentiated cells are due to their insensitivity to dox treatment. Most importantly, these results explain the heterogeneous, late onset and slow sunrise observed in undifferentiated cells and confirm that the induced XCI status in undifferentiated cells is determined by the two counteracting forces of XCI and XCR. Therefore, the established experimental system can be used as a unique tool to study both XCI and XCR. Manipulating genes involved in either XCI or XCR can tip the balance toward a predictable side.

The Roles of Histone Acetyltransferase Kat8 Protein Complex in XCR

Spen, a transcriptional repressor associated with histone deacetylase (HDAC) activities, was recently identified as a *Xist*-binding protein functionally important for *Xist*-mediated gene silencing (McHugh et al., 2015, Chu et al., 2015, Minajigi et al., 2015, Monfort et al., 2015, Moindrot et al., 2015). Therefore, we hypothesized that histone acetyltransferases (HATs) may be involved in XCR. To test this, we selected a few candidate HATs and their protein partners, which are expressed in undifferentiated ES cells (Figure S6). Short hairpin RNA (shRNA)-mediated knockdown of lysine acetyltransferase 8 (*Kat8*) and its protein partner male-specific lethal 2 (*Msl2*) significantly increased the killing effect of induced XCI in undifferentiated iXist cells (Figures 4A, 4B, and, S6). To rule out the off-targeting effect of shRNAs, we used a second shRNA against *Kat8* and *Msl2* and obtained similar results (Figure S7). A previous study showed that homozygous deletion of *Kat8* disrupts pluripotency, whereas the effect of heterozygous deletion was moderate and the mutant animals were largely normal (Li et al., 2012). To confirm that Kat8 and Msl2 are directly involved in XCR, we confirmed the shRNA knockdown of *Kat8* and *Msl2* (Figure S6) and showed that knocking down the candidate genes did not affect the expression of key pluripotency-related genes in the established cell lines (Figure S8). To further investigate the involvement of Kat8 and Msl2 in XCR, we examined *Xist* signals in live cells. shRNA against *Kat8* and *Msl2* helped to correct the late-onset and slow-growth sunrise behaviors in undifferentiated cells (Figures 4C and 4D). Meanwhile, shRNA *Msl2* also helped to slow down sunset in undifferentiated cells (Figure 4E). These results suggest that Kat8 and Msl2 are involved in XCR.

The Small Size of ΔA Mutant *Xist* Clouds

The sunrise behavior in undifferentiated cells during early hours of dox treatment is the outcome of a tug of war between XCI and XCR. Long hours of dox treatment unavoidably tip the balance toward XCI. *Xist* clouds could be observed in ~70%–90% of cells in all the established inducible *Xist* cell lines after a 24-hr dox treatment. We consider the *Xist* clouds observed at this stage as full-sized *Xist* signals. In wild-type cells, the *Xist* clouds are large and often associated with speckles scattered around a defined main territory covered by the cloud (Figure 5A). Interestingly, we noticed that the full-sized *Xist* clouds in ΔA mutants are significantly smaller and more compact compared with the wild-type clouds (Figures 5A–5C). We name this phenomenon "stopped budding." This observation holds true whether or not the cells were cultured as undifferentiated or differentiating cells (Figures 5B, 5C, and S9). We also generated cell lines in which A-repeat was deleted but not replaced with any exogenous sequences and obtained similar results (data not shown).

This result clarifies an issue regarding the ΔA *Xist* RNA signals. Based on RNA and DNA FISH techniques, it has been observed that, at the onset of XCI, the *Xist* RNA transcripts first form a silencing compartment (the core), which excludes the Pol II transcription machinery. At a later step, actively transcribed X-linked genes,

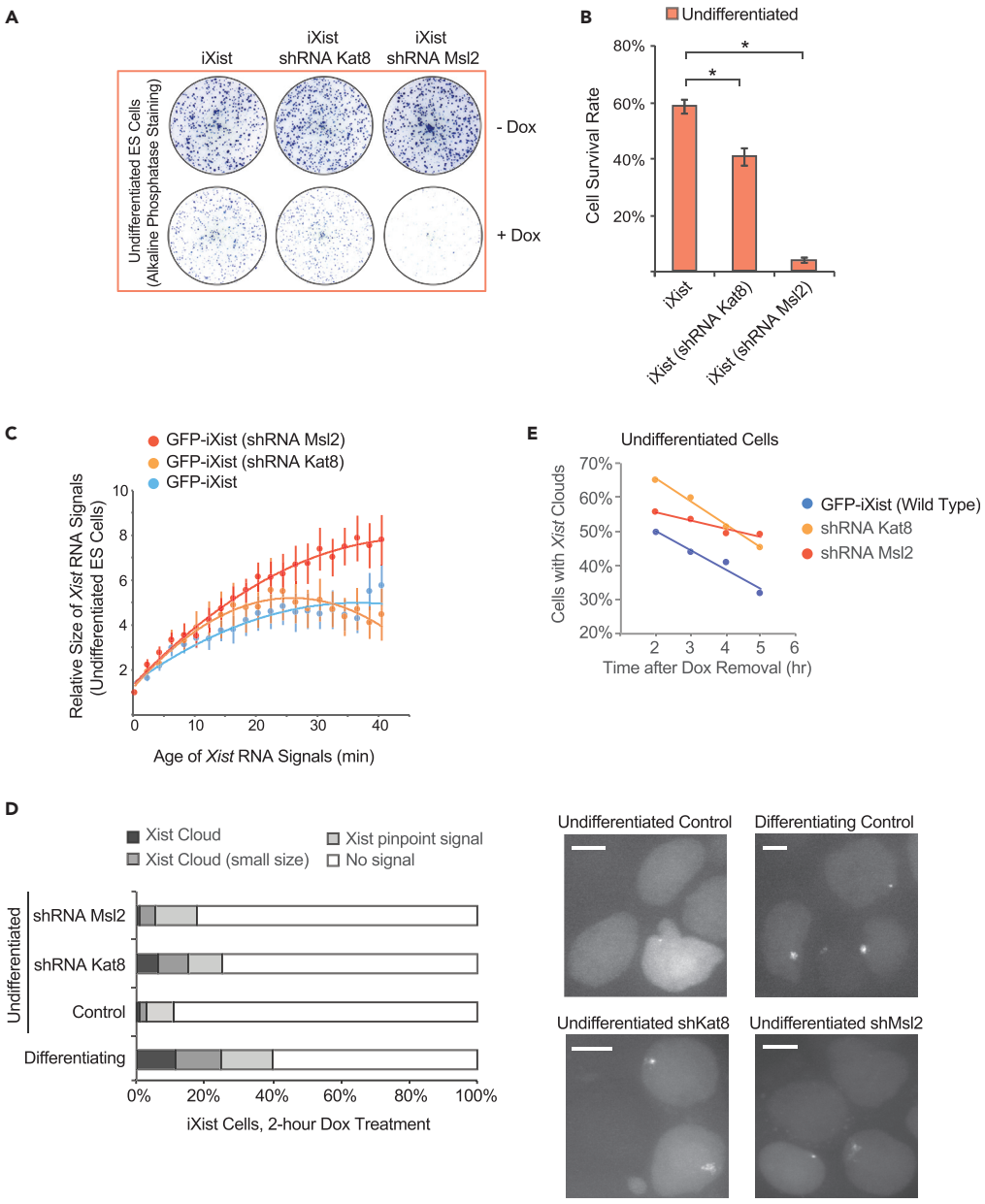

Figure 4. The Putative Roles of Histone Acetyltransferase Kat8 Protein Complex in XCR

(A and B) (A) Doxycycline-induced cell death assay on different inducible *Xist* cell lines. Cells were cultured as undifferentiated ES cells. Doxycycline treatment was carried out for 4 days. (B) Cell survival rate was calculated by alkaline phosphatase-stained colony counts. Data are shown as mean ± SEM of biological triplicate. The statistical analysis used is Student's *t* test. *$p < 0.05$.

(C) The growth curves of *Xist* RNA signals. The size (area) of a signal when it was first detected is defined as "size one" for the signal. *Xist* RNA signals were analyzed in 20 cells randomly selected from each sample. Data are shown as mean ± SEM with a trend line.

(D) *Xist* signals in live cells treated with dox for 2 hr. Representative images of *Xist* RNA signals in live cells after 2-hr dox treatment are shown as maximum intensity z projections. Scale bars, 5 μM.

(E) The rate of *Xist* RNA signal disappearance upon doxycycline removal. The cells were cultured as undifferentiated ES cells and treated with dox overnight before dox removal ($n > 175$ for the samples of each time point).

See also Figures S6–S8.

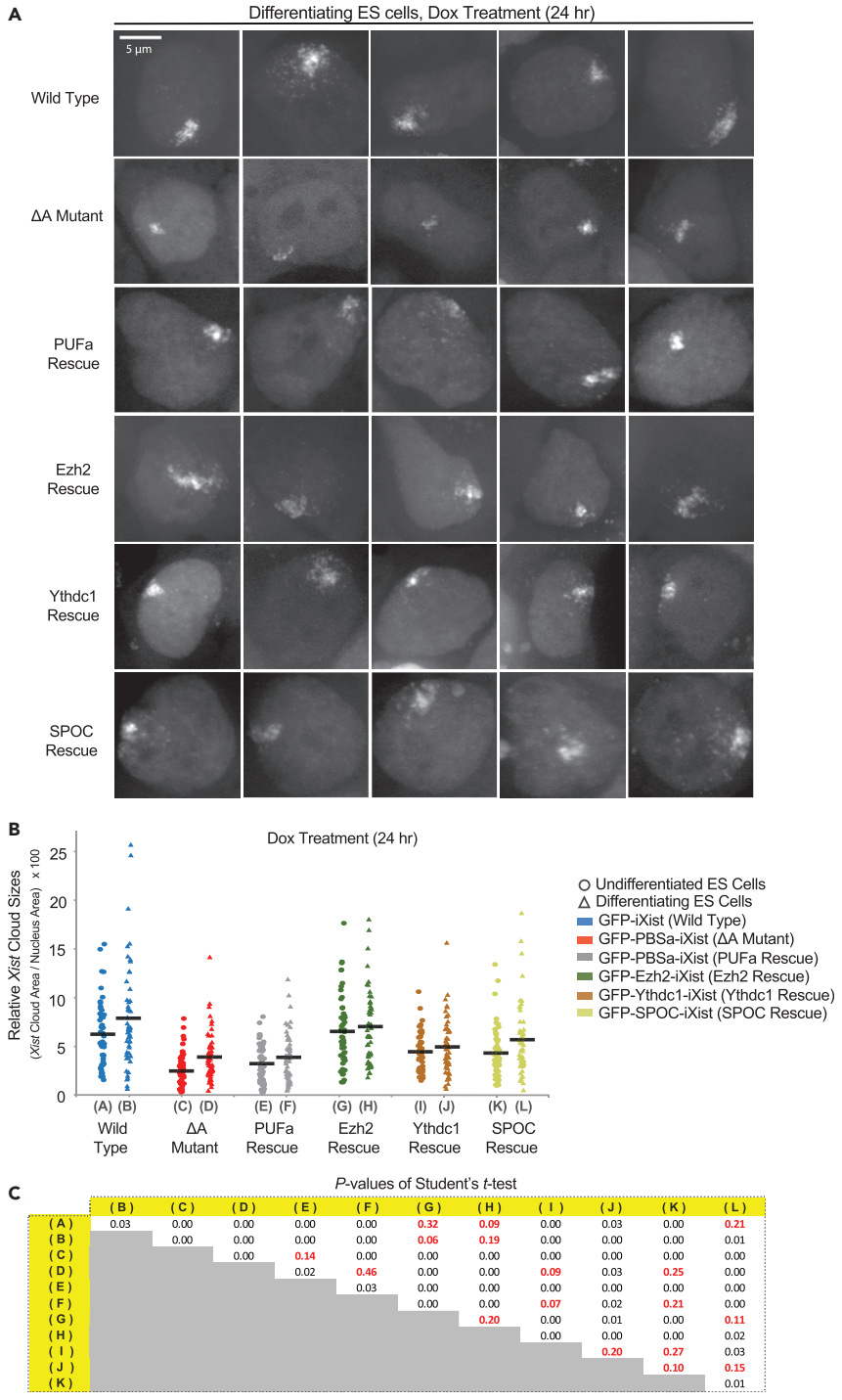

	(B)	(C)	(D)	(E)	(F)	(G)	(H)	(I)	(J)	(K)	(L)
(A)	0.03	0.00	0.00	0.00	0.00	0.32	0.09	0.00	0.03	0.00	0.21
(B)		0.00	0.00	0.00	0.00	0.06	0.19	0.00	0.00	0.00	0.01
(C)			0.00	0.14	0.00	0.00	0.00	0.00	0.00	0.00	0.00
(D)				0.02	0.46	0.00	0.00	0.09	0.03	0.25	0.00
(E)					0.03	0.00	0.00	0.00	0.00	0.00	0.00
(F)						0.00	0.00	0.07	0.02	0.21	0.00
(G)							0.20	0.00	0.01	0.00	0.11
(H)								0.00	0.00	0.00	0.02
(I)									0.20	0.27	0.03
(J)										0.10	0.15
(K)											0.01

Figure 5. The Small Size of ΔA Mutant *Xist* Clouds

(A) Representative images of *Xist* RNA signals in live cells. Images are shown as maximum intensity z projections. (B and C) (B) *Xist* cloud size measurement (n ≥ 50 for each dataset). Cells were cultured as differentiating ES cells. Doxycycline treatment was carried out for 24 hr. (C) Statistical analysis (Student's *t* test) was carried out to compare the *Xist* cloud size between all sample pairs within the experimental panel. p Values greater than 0.05 are labeled in red. See also Figure S9.

which are located outside or at the periphery of the compartment, are silenced (Chaumeil et al., 2006). The formation of silencing core does not depend on A-repeat, but the later step does. Recently, genomic mapping results further provided direct evidence that the ΔA mutant *Xist* transcripts could not efficiently cover actively transcribed genes (Engreitz et al., 2013). Based on these results, it is straightforward to assume that the ΔA *Xist* cloud should have a smaller size than the wild-type, because it only covers the silencing core but has difficulties to reach out to efficiently cover the actively transcribed genes located at the peripheral region. However, possibly because of the technical limitations of RNA FISH, it was concluded that the appearances of *Xist* clouds were "comparable" between the wild-type and the ΔA mutant (Chaumeil et al., 2006; Wutz et al., 2002; Engreitz et al., 2013), even though undersized ΔA mutant *Xist* clouds can be seen in the published data (Engreitz et al., 2013). Our live-cell imaging experiments clarify this issue, and the results fit in more comfortably with the previous observations.

Artificial Tethering of Ezh2 Restored the Attenuated PRC Activities along the ΔA Mutant *Xist* RNA

In our experimental system, PUFa can be fused with individual candidate proteins and tethers the protein back onto the ΔA mutant *Xist* transcripts to dissect the *Xist* functionality. Three candidate proteins (Ezh2, Spen, and Ythdc1) were selected for this study. Unfortunately, we encountered difficulties in generating the large DNA constructs of SPEN (~3,700 amino acids). Spen (split end), as its name suggests, contains two functional domains separated by a large linker region (Ariyoshi and Schwabe, 2003). The two functional domains are the N-terminal RNA binding domain and the SPOC domain (Spen paralog and ortholog C terminal). It is a reasonable assumption that SPOC is the critical functional domain directly involved in XCI. We, therefore, tethered the SPOC domain onto the ΔA mutant transcripts. Artificial tethering of Ezh2, SPOC, and Ythdc1 all partially rescued the "stopped budding" mutant phenotype, whereas Ezh2 clearly showed the most significant rescue effect among the three (Figures 5A–5C). This result shows that Ezh2 is functionally related to *Xist* RNA spreading. To assess the functionality of *Xist*-mediated gene silencing, we measured the killing effect of induced XCI (Figure 6A). The results show that GFP-iXist is functionally equivalent to the wild-type iXist. Replacing of A-repeat with PBSa in GFP-PBSa-iXist (ΔA mutant) clearly disrupted the *Xist*-mediated gene silencing (Figure 6A). This mutant phenotype was significantly rescued by artificially tethering any of the three candidate proteins onto the mutant *Xist* transcripts (Figure 6A). Other than the killing effect, we also examined the direct effect of Ezh2 tethering on X-linked gene expression. The results confirm that Ezh2 tethering helped to restore the capacity of *Xist*-mediated gene silencing (Figure S10). To confirm that the observed rescue effect is due to the tethering of the candidate proteins onto the deleted A-repeat region but not the two endogenous PBSa sites along *Xist*, we overexpressed Ezh2-PUFa in cells carrying a *Xist* transgene untagged with PBSa (Figure S11A). Induced *Xist* expression in these cells showed a killing effect comparable to the iXist control cells. This result shows that the possible interaction between Ezh2-PUFa and the two endogenous PBSa sites within *Xist* did not generate a detectable effect in the cell killing assay (Figure S11A). Moreover, when Ezh2-PUFa overexpression was uncoupled from the induced *Xist* expression, Ezh2 overexpression alone was not able to silence the neomycin resistance gene and generate a detectable effect on cell growth (Figure S11B). Taken together, these results show that Ezh2 is important for both *Xist* RNA spreading and *Xist*-mediated gene silencing. Ythdc1 and SPOC play more specialized roles in *Xist*-mediated gene silencing.

It is known that PRC proteins play important roles in establishing the repressive chromatin states in XCI (Brockdorff, 2017). There are two major PRCs, PRC1 and PRC2. PRC1 catalyzes mono-ubiquitylation of histone H2A lysine 119 (H2AK119u1). Ezh2 is the enzyme of the PRC2 complex, which methylates histone H3 lysine 27 (H3K27me3). Currently, how PRC activities are recruited in XCI is under debate. One hypothesis is that PRC2 is recruited through the direct interaction between Ezh2 and *Xist* (Zhao et al., 2008). The other hypothesis is that the PRC1 activity recruits PRC2 (Almeida et al., 2017). To study the PRC activities in XCI, we performed immunostaining to detect H3K27me3 and H2AK119ub enrichment along Xi. Interestingly, different from what is reported in the supplementary section of a previous literature (Almeida et al., 2017), we observed that the PRC activities (H3K27me3 and H2AK119ub enrichment) were significantly attenuated in ΔA mutant (Figure 6B). This result shows that the A-repeat is involved in recruiting or spreading PRC activities. Artificial tethering of Ezh2 onto the ΔA mutant *Xist* transcripts significantly restored not only the H3K27me3 enrichment but also the H2AK119ub enrichment (Figure 6B). This result confirms, regardless of whether PRC2 is recruited in XCI through PRC1 in the first place, the synergetic mechanism between PRC1 and PRC2: one helps to recruit the other (Almeida et al., 2017).

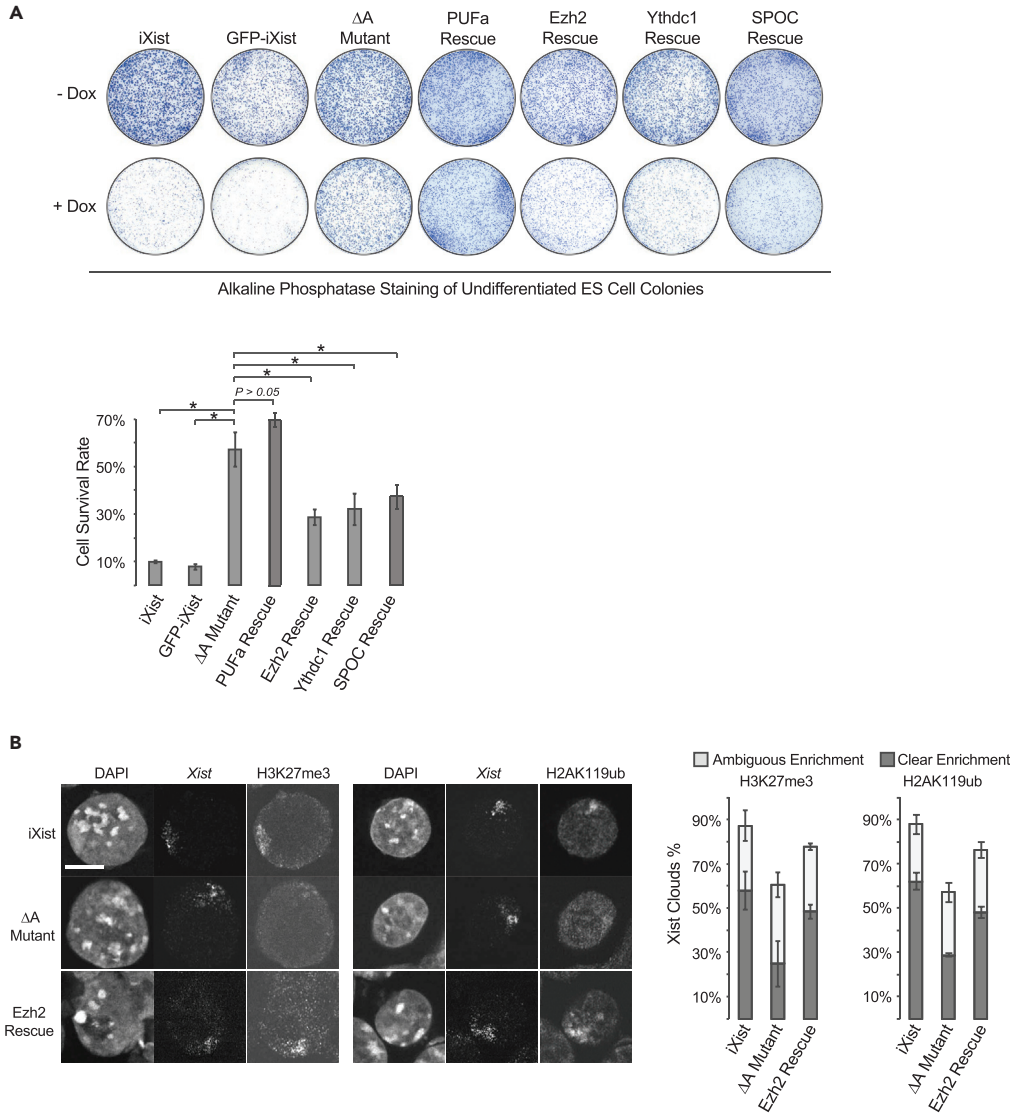

Figure 6. Artificial Tethering of Ezh2 Restored the Attenuated PRC Activities along the ΔA Mutant *Xist* RNA

(A) Functional validation of the inducible *Xist* alleles by doxycycline-induced cell death. Cells were cultured as undifferentiated ES cells. Doxycycline treatment was carried out for 5 days. Cell survival rate was calculated by measuring area stained by alkaline phosphatase staining. Data are shown as mean ± SEM of biological triplicate. The statistical analysis used is Student's *t* test. The cell survival rate of ΔA mutant was compared with the other 4 samples. *p < 0.05.

(B) Immuno-RNA FISH to detect H3K27me3, H2AK119ub, and *Xist* in cells, which were differentiated and treated with dox for 48 hr. The immunostains were performed before the RNA FISH. DNA was counterstained with DAPI. Data are shown as mean ± SD of biological triplicate (n = 63–153 for each sample). Scale bar, 5 μM.

See also Figures S10 and S11.

DISCUSSION

The Pumilio-Based System Provides Both a Label and an Effector in Studying Long Non-coding RNAs

In summary, the Pumilio-based labeling system we report here enables high-quality live-cell imaging of *Xist* RNA and provides insightful details into the RNA's behavior in live cells. Utilizing a second PBS to artificially tether candidate proteins onto *Xist* provides a "second handle" in the system, which helps to dissect the functional mechanisms underlying XCI. This approach can be applied to study other RNAs, in particular long non-coding RNAs.

Inducible XCI in Undifferentiated ES Cells Provides a Tool to Study Both XCI and XCR

XCI and XCR are two excellent biological events for studying epigenetic mechanisms. As opposed to XCI, XCR is poorly investigated. Two waves of XCR occur during the natural life cycle of a mouse, blastocyst formation and primordial germ cell specification (Ohhata and Wutz, 2013), which are two embryonic developmental events difficult to be recapitulated *in vitro*. XCR also occurs in the artificial experimental system of induced pluripotent stem cell (iPSC) formation (Ohhata and Wutz, 2013), which is a slow, sporadic, and heterogeneous event less favorable for detailed studies on XCR. In this study, we show that the induced XCI status in undifferentiated cells is the balanced outcome of two counteracting forces, XCI and XCR. Genetic manipulation on related genes may tip the balance toward a predictable direction. Using this unique experimental system, we identify Kat8 and Msl2, two proteins of *Drosophila* dosage compensation responsible for enhancing the gene transcription from the single X chromosome in males (Lucchesi and Kuroda, 2015), as two players involved in mammalian XCR.

The observed "star" behavior of sunrise in undifferentiated cells indicates an underlying mechanism preventing *Xist* cloud formation. Whether Kat8 and Msl2 are directly involved in *Xist* cloud formation remains to be elucidated by future studies. It should also be noted that Kat8 expression may not be perfectly restricted in undifferentiated ES cells. Although Western blot results have shown that the protein level of Kat8 is sharply down-regulated during *in vitro* differentiation of ES cells (Li et al., 2012), our quantitative RT-PCR data did not detect the similar pattern at the RNA level (data not shown). However, somatic expression of a gene cannot rule out the gene's role in XCR. We believe XCI is achieved through multiple layers of epigenetic modifications. In theory, genes involved in reactivating the "inner" layers of epigenetic silencing may still be expressed in somatic cells without reactivating the silenced X chromosome. Meanwhile, it would be interesting to manipulate the expression level of Kat8 and Msl2 in female cells (ES cells, somatic cells, or iPSCs) to study their effect on XCI.

A previous study showed that Kat8-associated protein complexes positively regulate *Tsix* expression and, as a consequence, repress *Xist* expression (Chelmicki et al., 2014). It is known that *Tsix* counteracts *Xist* through the action of antisense transcription across the gene body of *Xist* (Shibata and Lee, 2004; Luikenhuis et al., 2001). The inducible *Xist* transgene involved in this study does not contain the 5′ region of *Tsix*, including the gene's promoter (Figure S12). Moreover, the *Xist* transgene is controlled by a doxycycline-inducible promoter and located ~50 Mb away from the endogenous *Tsix* gene. We performed RT-PCR and confirmed that no antisense transcription occurs along the 5′ region of the inducible *Xist* transgene (Figure S12).

Other than the intrinsic XCR, the difficulties of sunrise in undifferentiated cells could also be explained by the shortage of resources required in XCI, which are only up-regulated upon differentiation. The two possibilities are not mutually exclusive. The results of sunset experiments help to confirm that the XCR is one reason behind the difficulties of sunrise in undifferentiated cells, but do not rule out the other possibility.

Functional Dissection of *Xist*: Spreading versus Silencing

Artificially recruiting Ezh2, SPOC, and Ythdc1 onto the ΔA mutant *Xist* transcripts showed the effects of all three proteins on both *Xist* RNA spreading and *Xist*-mediated gene silencing, whereas Ezh2 showed the most significant role in *Xist* RNA spreading among the three. With little effect on rescuing the *Xist* RNA spreading defect, artificially recruiting Ythdc1 alone or SPOC alone significantly restored the killing effect. This result can be explained by the neomycin resistance gene located close to the inducible *Xist* transgene. A significant fraction of cell death caused by induced XCI is due to *Xist*-mediated silencing of the nearby neomycin-resistant gene. We carried out control experiments and confirmed that the silencing of the nearby neomycin-resistant gene was mediated by *Xist*, as the Ezh2 transgene showed no detectable effect when its expression was uncoupled from the induced *Xist* expression (Figure S11).

Technical Limitation of DNA/RNA FISH: Sensitivity versus Specificity

A variety of approaches are used in RNA or DNA FISH to increase the signal specificity. For example, a high concentration of Cot-1 DNA is mixed with the FISH probes to block unspecific hybridization. As junk DNA, the unlabeled Cot-1 DNA helps to increase the detection specificity, but it unavoidably decreases the detection resolution and sensitivity. In this study, our live-cell imaging experiments clearly revealed the small size of the ΔA mutant *Xist* clouds. We believe the small and compact *Xist* clouds observed in the ΔA mutant are *Xist* RNAs covering the silencing core. For the wild-type *Xist* clouds, we believe many

speckles, if not all, that scattered from the main territory of an *Xist* cloud are *Xist* RNAs associated with actively transcribed genes positioned further away from the main territory. Indeed, the results of RNA polymerase II (Pol II) immunostaining show that the silencing core territory devoid of Pol II staining is smaller than the territory marked by iXist-GFP (Figure S13). In fact, the scattered appearance of the wild-type *Xist* clouds is occasionally seen in RNA FISH (data not shown). Similarly, DNA FISH on X-linked genes occasionally detects a gene located "far away" from a *Xist* cloud detected in RNA FISH or a "chromosome territory" detected by chromosome paint probes in DNA FISH (Chen et al., 2016). However, no specific interpretation has been made on these observations. We believe many actively transcribed X-linked genes are located outside of the "chromosome territory" defined by the *Xist* RNA FISH signals or the chromosome paint DNA FISH signals. The scattered appearance of *Xist* clouds clearly detected in live-cell imaging indicates *Xist* RNAs spreading out to cover the actively transcribed genes, which are located not only at the periphery of the main territory of a *Xist* cloud but also farther away from it. How *Xist* RNA spreads out and precisely covers X-linked genes that are actively transcribed from its host chromosome and located "far away" from the main chromosome territory awaits future studies.

Technical Limitations of the Study

It is noticeable that the experimental system of this study has its own technical limitations. The "wild-type" *Xist* in this study is an induced transgene in male cells located at the *Hprt* locus carrying PBSb tags on its 5′ end. Its behavior may not be identical to that of the endogenous *Xist* in female cells. However, all the foregoing artificial features are commonly shared by the "wild-type" and the mutant *Xist*, in undifferentiated and differentiating cells. The comparison between the "wild-type" and the mutant and the comparison between undifferentiated and differentiating cells help to reveal the biological insights, as the observed differences cannot be attributed to the artificial features commonly shared by all parties.

It should be also noticed that, with the secondary structure of *Xist* largely unknown, any tagging of the RNA has the potential risk of disrupting the RNA's putative secondary structure. However, it is unlikely that the long RNA forms a single rigid secondary structure. In a study using a serial deletion approach to functionally dissect *Xist*, A-repeat was identified as the single most critical domain for the *Xist* functionality (Wutz et al., 2002). This result argues against the possibility that the full-length *Xist* RNA forms a scaffold with a rigid structure. Indeed, it is hypothesized that *Xist* functions as a malleable scaffold with modular and swappable functional domains (Guttman and Rinn, 2012). Based on current research, A-repeat may form its own structural domain independent from the remaining parts of the long RNA (Liu et al., 2017). Therefore, replacing A-repeat with PBS may not affect the global secondary structure of the long *Xist* RNA. Sequence wise, the A-repeat region consists of 7.5 sequence repeats (Brockdorff et al., 1992). Structure wise, the region may form an elaborated secondary structure in which the sequence repeats behave differently in forming different structural units (Liu et al., 2017). How the structural units recruit proteins and how many copies of each protein are recruited by the structural units remain unknown. In this study, we assumed that each sequence repeat recruits one copy of the candidate protein and used 10 copies of PBSa to replace the A-repeat region. In theory, 10 copies of each target protein can be tethered onto each RNA transcript maximally. The actual amount of each candidate protein recruited onto each RNA transcript in this study may differ from the endogenous situation and can be further optimized in future studies.

Xist is a long RNA with the critical functional domain near its 5′ end. In theory, the live-cell imaging tag can be placed either at the 5′ or 3′ end of the RNA. Tagging at the 3′ end may prevent the imaging tag from interfering with the functional domain of *Xist*. On the other hand, 3′ tagging may not allow the system to closely monitor the RNA's behavior in live cells. Labeling at the 5′ end provides the opposite advantage and disadvantage. In this study, we chose 5′ tagging, because we encountered technical difficulties in generating the DNA constructs of 3′ tagging. Our data show that the *Xist* functionality remains largely intact with 5′ tagging.

In live-cell imaging, the length of the observation time window is limited to 2–3 hr due to technical issues, such as photobleaching, cell tracing, re-focusing, and stage drifting.

METHODS

All methods can be found in the accompanying Transparent Methods supplemental file.

SUPPLEMENTAL INFORMATION

Supplemental Information includes Transparent Methods, 13 figures, and 4 videos and can be found with this article online at https://doi.org/10.1016/j.isci.2018.09.007.

ACKNOWLEDGMENTS

We thank Su I-Hsin for the mouse *Ezh2* cDNA. This work was supported by Singapore Ministry of Education Academic Research Fund (MOE2015-T2-1-093) and by the Singapore National Research Foundation under its Cooperative Basic Research Grant administered by the Singapore Ministry of Health's National Medical Research Council (NMRC/CBRG/0093/2015).

AUTHOR CONTRIBUTIONS

L-F.Z. conceived the idea. L.C. and L-F.Z. designed the experiments. N.H. performed the majority of the experiments. S.P.Y.V., Y.Z., and L-T.L. performed shRNA knockdown experiments. R.C. established the iXist cell line. N.H., L.C., and L-F.Z. analyzed and interpreted the data. S-K.L. and H-Y.L. provided technical assistance on Airyscan microscopy. A.L. and S.S. provided technical support for spinning disk confocal microscopy. L.C. and L-F.Z. wrote the manuscript.

DECLARATION OF INTERESTS

The authors declare no competing interests.

Received: July 4, 2018
Revised: September 4, 2018
Accepted: September 7, 2018
Published: October 26, 2018

REFERENCES

Almeida, M., Pintacuda, G., Masui, O., Koseki, Y., Gdula, M., Cerase, A., Brown, D., Mould, A., Innocent, C., Nakayama, M., et al. (2017). PCGF3/5-PRC1 initiates Polycomb recruitment in X chromosome inactivation. Science *356*, 1081–1084.

Ariyoshi, M., and Schwabe, J.W. (2003). A conserved structural motif reveals the essential transcriptional repression function of Spen proteins and their role in developmental signaling. Genes Dev. *17*, 1909–1920.

Brockdorff, N. (2017). Polycomb complexes in X chromosome inactivation. Philos. Trans. R. Soc. Lond. B Biol. Sci. *372*, 20170021.

Brockdorff, N., Ashworth, A., Kay, G.F., Mccabe, V.M., Norris, D.P., Cooper, P.J., Swift, S., and Rastan, S. (1992). The product of the mouse Xist gene is a 15 kb inactive X-specific transcript containing no conserved ORF and located in the nucleus. Cell *71*, 515–526.

Cao, R., Wang, L., Wang, H., Xia, L., Erdjument-Bromage, H., Tempst, P., Jones, R.S., and Zhang, Y. (2002). Role of histone H3 lysine 27 methylation in Polycomb-group silencing. Science *298*, 1039–1043.

Chambers, I., Silva, J., Colby, D., Nichols, J., Nijmeijer, B., Robertson, M., Vrana, J., Jones, K., Grotewold, L., and Smith, A. (2007). Nanog safeguards pluripotency and mediates germline development. Nature *450*, 1230–1234.

Chaumeil, J., Le Baccon, P., Wutz, A., and Heard, E. (2006). A novel role for Xist RNA in the formation of a repressive nuclear compartment into which genes are recruited when silenced. Genes Dev. *20*, 2223–2237.

Chelmicki, T., Dundar, F., Turley, M.J., Khanam, T., Aktas, T., Ramirez, F., Gendrel, A.V., Wright, P.R., Videm, P., Backofen, R., et al. (2014). MOF-associated complexes ensure stem cell identity and Xist repression. Elife *3*, e02024.

Chen, C.K., Blanco, M., Jackson, C., Aznauryan, E., Ollikainen, N., Surka, C., Chow, A., Cerase, A., Mcdonel, P., and Guttman, M. (2016). Xist recruits the X chromosome to the nuclear lamina to enable chromosome-wide silencing. Science *354*, 468–472.

Cheng, A.W., Jillette, N., Lee, P., Plaskon, D., Fujiwara, Y., Wang, W., Taghbalout, A., and Wang, H. (2016). Casilio: a versatile CRISPR-Cas9-Pumilio hybrid for gene regulation and genomic labeling. Cell Res. *26*, 254–257.

Cheong, C.G., and Hall, T.M. (2006). Engineering RNA sequence specificity of Pumilio repeats. Proc. Natl. Acad. Sci. USA *103*, 13635–13639.

Chu, C., Zhang, Q.C., da Rocha, S.T., Flynn, R.A., Bharadwaj, M., Calabrese, J.M., Magnuson, T., Heard, E., and Chang, H.Y. (2015). Systematic discovery of Xist RNA binding proteins. Cell *161*, 404–416.

Clemson, C.M., Mcneil, J.A., Willard, H.F., and Lawrence, J.B. (1996). XIST RNA paints the inactive X chromosome at interphase: evidence for a novel RNA involved in nuclear/chromosome structure. J. Cell Biol. *132*, 259.

Engreitz, J.M., Pandya-Jones, A., Mcdonel, P., Shishkin, A., Sirokman, K., Surka, C., Kadri, S., Xing, J., Goren, A., Lander, E.S., et al. (2013). The Xist lncRNA exploits three-dimensional genome architecture to spread across the X chromosome. Science *341*, 1237973.

Guttman, M., and Rinn, J.L. (2012). Modular regulatory principles of large non-coding RNAs. Nature *482*, 339–346.

Kyba, M., Perlingeiro, R.C., and Daley, G.Q. (2002). HoxB4 confers definitive lymphoid-myeloid engraftment potential on embryonic stem cell and yolk sac hematopoietic progenitors. Cell *109*, 29–37.

Li, X., Li, L., Pandey, R., Byun, J.S., Gardner, K., Qin, Z., and Dou, Y. (2012). The histone acetyltransferase MOF is a key regulator of the embryonic stem cell core transcriptional network. Cell Stem Cell *11*, 163–178.

Liu, F., Somarowthu, S., and Pyle, A.M. (2017). Visualizing the secondary and tertiary architectural domains of lncRNA RepA. Nat. Chem. Biol. *13*, 282–289.

Lucchesi, J.C., and Kuroda, M.I. (2015). Dosage compensation in Drosophila. Cold Spring Harb. Perspect. Biol. *7*, https://doi.org/10.1101/cshperspect.a019398.

Luikenhuis, S., Wutz, A., and Jaenisch, R. (2001). Antisense transcription through the Xist locus mediates Tsix function in embryonic stem cells. Mol. Cell. Biol. *21*, 8512–8520.

McHugh, C.A., Chen, C.K., Chow, A., Surka, C.F., Tran, C., Mcdonel, P., Pandya-Jones, A., Blanco, M., Burghard, C., Moradian, A., et al. (2015). The Xist lncRNA interacts directly with SHARP to

silence transcription through HDAC3. Nature *521*, 232–236.

Minajigi, A., Froberg, J.E., Wei, C., Sunwoo, H., Kesner, B., Colognori, D., Lessing, D., Payer, B., Boukhali, M., Haas, W., and Lee, J.T. (2015). Chromosomes. A comprehensive Xist interactome reveals cohesin repulsion and an RNA-directed chromosome conformation. Science *349*, aab2276.

Moindrot, B., Cerase, A., Coker, H., Masui, O., Grijzenhout, A., Pintacuda, G., Schermelleh, L., Nesterova, T.B., and Brockdorff, N. (2015). A pooled shRNA screen identifies Rbm15, spen, and Wtap as factors required for xist RNA-mediated silencing. Cell Rep. *12*, 562–572.

Monfort, A., Di Minin, G., Postlmayr, A., Freimann, R., Arieti, F., Thore, S., and Wutz, A. (2015). Identification of spen as a crucial factor for xist function through forward genetic screening in haploid embryonic stem cells. Cell Rep. *12*, 554–561.

Ng, K., Daigle, N., Bancaud, A., Ohhata, T., Humphreys, P., Walker, R., Ellenberg, J., and Wutz, A. (2011). A system for imaging the regulatory noncoding Xist RNA in living mouse embryonic stem cells. Mol. Biol. Cell *22*, 2634–2645.

Ohhata, T., and Wutz, A. (2013). Reactivation of the inactive X chromosome in development and reprogramming. Cell. Mol. Life Sci. *70*, 2443–2461.

Patil, D.P., Chen, C.K., Pickering, B.F., Chow, A., Jackson, C., Guttman, M., and Jaffrey, S.R. (2016). m(6)A RNA methylation promotes XIST-mediated transcriptional repression. Nature *537*, 369–373.

Payer, B., and Lee, J.T. (2008). X chromosome dosage compensation: how mammals keep the balance. Annu. Rev. Genet. *42*, 733–772.

Plath, K., Fang, J., Mlynarczyk-Evans, S.K., Cao, R., Worringer, K.A., Wang, H., De La Cruz, C.C., Otte, A.P., Panning, B., and Zhang, Y. (2003). Role of histone H3 lysine 27 methylation in X inactivation. Science *300*, 131–135.

Shibata, S., and Lee, J.T. (2004). Tsix transcription- versus RNA-based mechanisms in Xist repression and epigenetic choice. Curr. Biol. *14*, 1747–1754.

Urbanek, M.O., Galka-Marciniak, P., Olejniczak, M., and Krzyzosiak, W.J. (2014). RNA imaging in living cells - methods and applications. RNA Biol. *11*, 1083–1095.

Wang, X., Mclachlan, J., Zamore, P.D., and Hall, T.M. (2002). Modular recognition of RNA by a human pumilio-homology domain. Cell *110*, 501–512.

Wutz, A., Rasmussen, T.P., and Jaenisch, R. (2002). Chromosomal silencing and localization are mediated by different domains of Xist RNA. Nat. Genet. *30*, 167–174.

Zhao, J., Sun, B.K., Erwin, J.A., Song, J.J., and Lee, J.T. (2008). Polycomb proteins targeted by a short repeat RNA to the mouse X chromosome. Science *322*, 750–756.

ISCI, Volume *8*

Supplemental Information

Live-Cell Imaging and Functional Dissection of *Xist* RNA Reveal Mechanisms of X Chromosome Inactivation and Reactivation

Norbert Ha, Lan-Tian Lai, Rosi Chelliah, Yashu Zhen, Seet Pei Yi Vanessa, Soak-Kuan Lai, Hoi-Yeung Li, Alexander Ludwig, Sara Sandin, Lingyi Chen, and Li-Feng Zhang

Supplemental Information

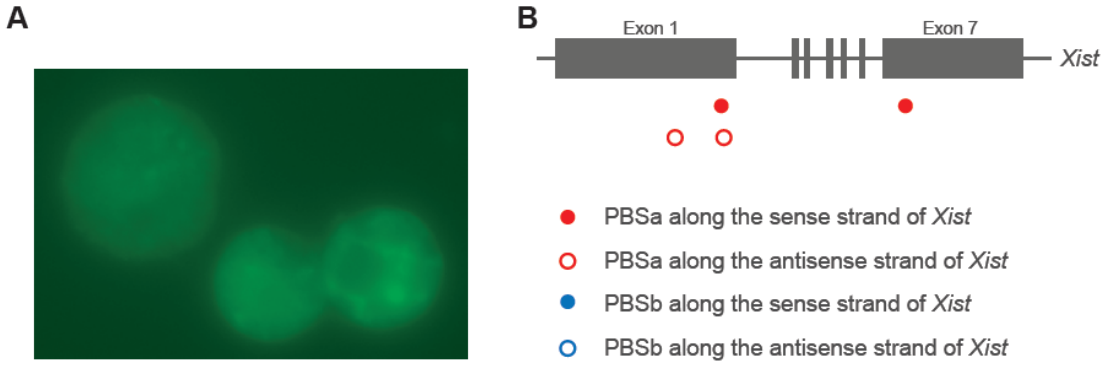

Figure S1: The cross-reactivity of PUFa / PBSb and the PBSa sites identified in the endogenous sequence of *Xist* (Related to Figure 1). (A) The inducible *Xist* transgene carries 25 copies of PBSb at its 5' end. The cells were transiently transfected with a plasmid carrying a PUFa-EGFP fusion gene. The transfected cells were treated with dox for 24 hours. A live-cell image of the GFP channel is shown. The image was taken using a wide-field fluorescent microscope. No *Xist* signals were detected from the entire cell population, which confirms no cross-reactivity between PUFa and PBSb. **(B)** A map of *Xist* gene with the PBSa sites identified in its endogenous sequence.

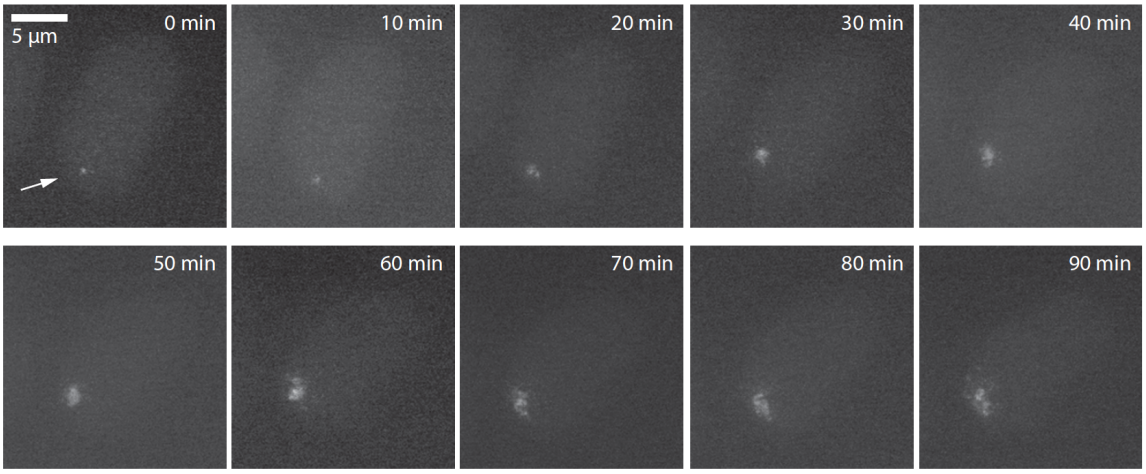

Figure S2: The emergence of an *Xist* RNA signal upon dox induction (Related to Figure 2). The emergence of an *Xist* RNA signal in a differentiating ES cell. Images are shown in a 90-min time span with a 10-min time interval. The time point when the signal was first detected is defined as time zero. Maximum intensity z-projections are shown.

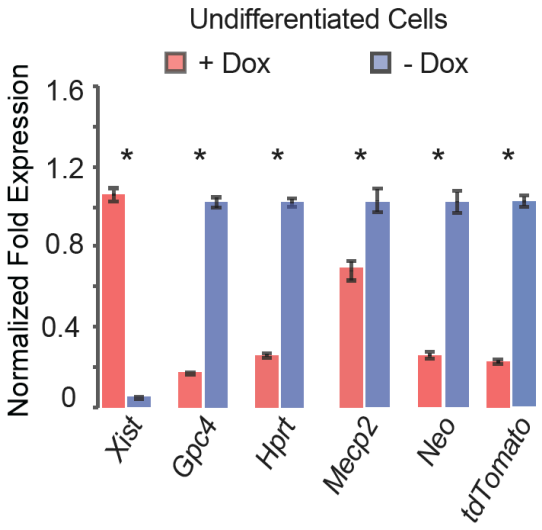

Figure S3: Quantitative RT-PCR results to show the effect of induced *Xist* expression on X-linked genes in undifferentiated cells (Related to Figure 3). Dox treatment was carried out for 24 hours. The results are shown in relative fold expression. Normalization was performed using *Actb* and *Gapdh*. Error bars indicate SEM (n = 3). The statistical analysis used is the Student's t-test. One asterisk indicates *P*-value smaller than 0.05.

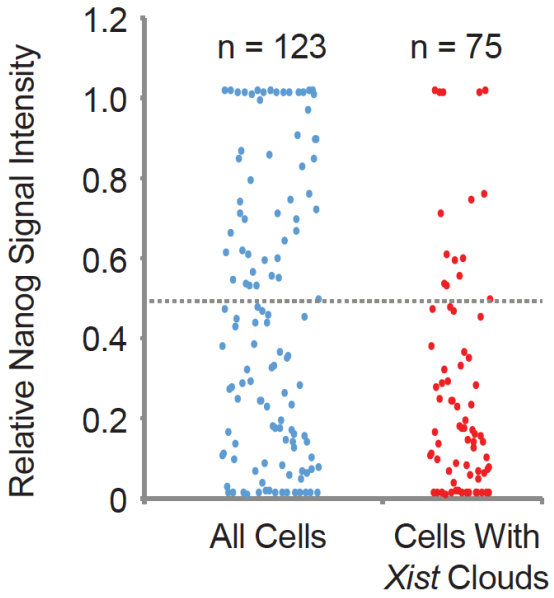

Figure S4: Measurement of Nanog signal intensity (Related to Figure 3).

Immuno-RNA FISH to detect Nanog and *Xist* in undifferentiated iXist cells treated with dox for 3 hours. Cells were cultured in the conventional Lif-containing ES culture medium without 2i. Nanog was detected by immunostain. The mean Nanog signal intensity in each cell was measure by ImageJ. To normalize the signal intensity variance among difference microscope images, the cells within one image were ranked according to the mean Nanog signal intensity within each cell. The cell with the highest ranking was scored 1 for its "Relative Nanog Signal Intensity". The cell with the lowest ranking was scored 0. The rest of the cells from the same image were scored between 1 and 0 proportionally according to each cell's mean Nanog signal intensity. The relative Nanog signal intensity value 0.5 is marked by a dashed line.

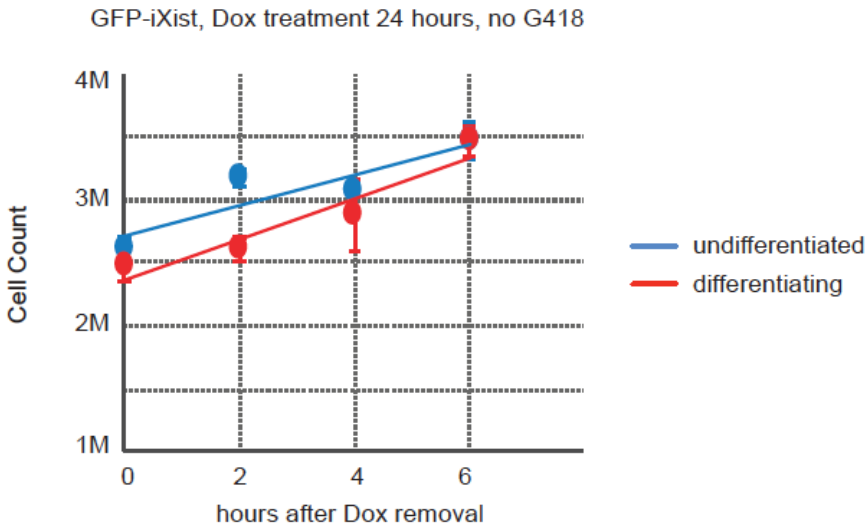

Figure S5: The growth curves of GFP-iXist cells during the 6-hour time window after Dox removal (Related to Figure 3). Data are shown as mean ± S.D. of biological triplicate.

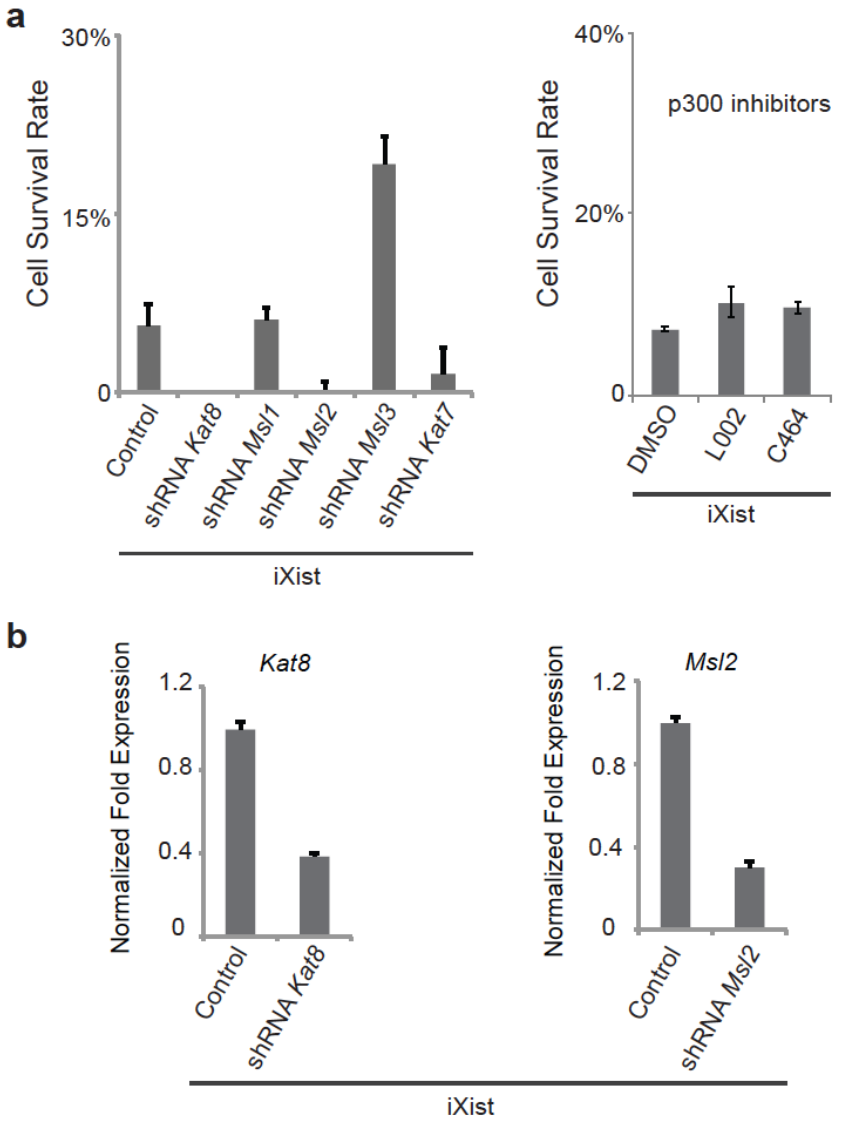

Figure S6: Test on the involvement of histone acetyltransferase candidate proteins in XCR (Related to Figure 4). (a) Doxycycline-induced cell death assay was carried out on iXist cells. The cells were either treated with chemical inhibitors for p300 or transfected with shRNAs against different candidate

proteins. Dox treatment was carried out for 4 days. Data are shown as mean ± S.E.M of biological triplicate. Note: The cell survival rates were calculated based on hemocytometer cell count, which has more experimental error than alkaline phosphatase staining. **(b)** Quantitative RT-PCR to validate the effects of shRNA knocking-down. Data are shown in relative fold expression. Normalization was performed using *Actb* and *Gapdh*. Error bars indicate SEM (n = 3).

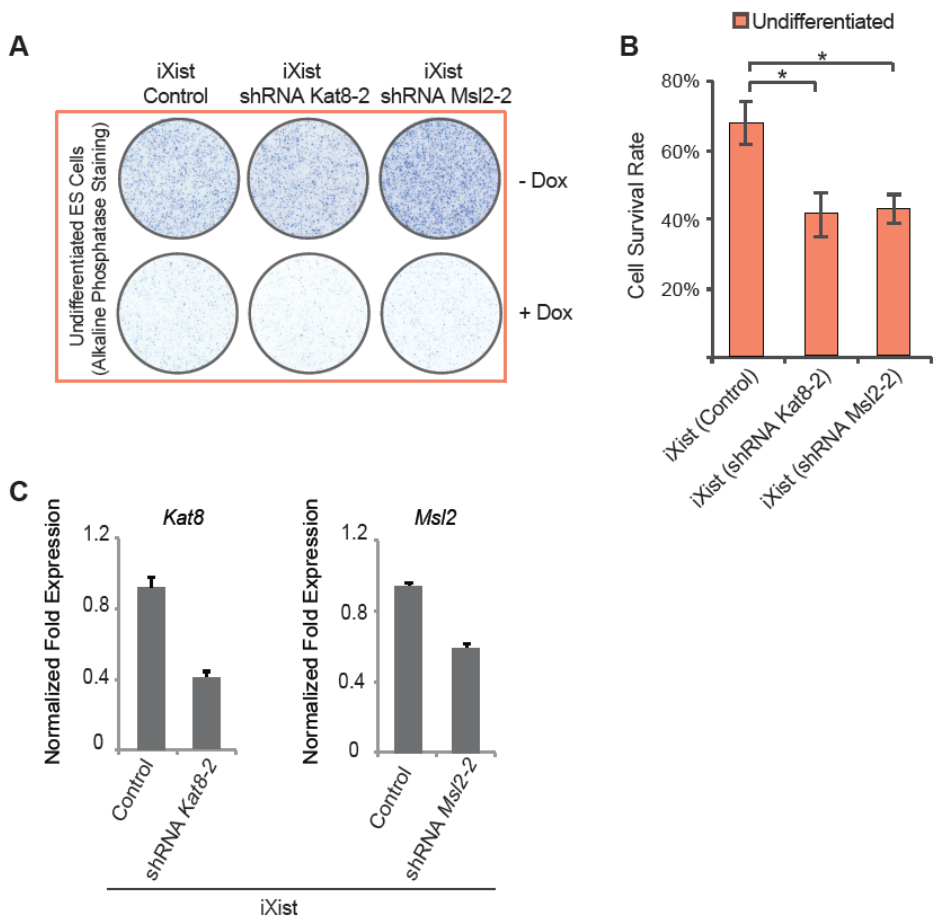

Figure S7: Using a 2nd shRNA against *Kat8* and *Msl2* to rule out the shRNA off-targeting effect (Related to Figure 4). (A, B) Doxycycline-induced cell death assay on different inducible *Xist* cell lines. Cells were cultured as undifferentiated ES cells. Dox treatment was carried out for 4 days. Cell survival rate was calculated by AP stained colony counts. *Data* are *shown* as mean ± S.E.M of biological triplicate. The statistical analysis used is the Student's *t*-test. One asterisk indicates *P*-value smaller than 0.05. **(C)** Quantitative RT-PCR to validate the effects of shRNA knocking-down. Data are shown in relative fold expression. Normalization was performed using *Actb* and *Gapdh*. Error bars indicate SEM (n = 3).

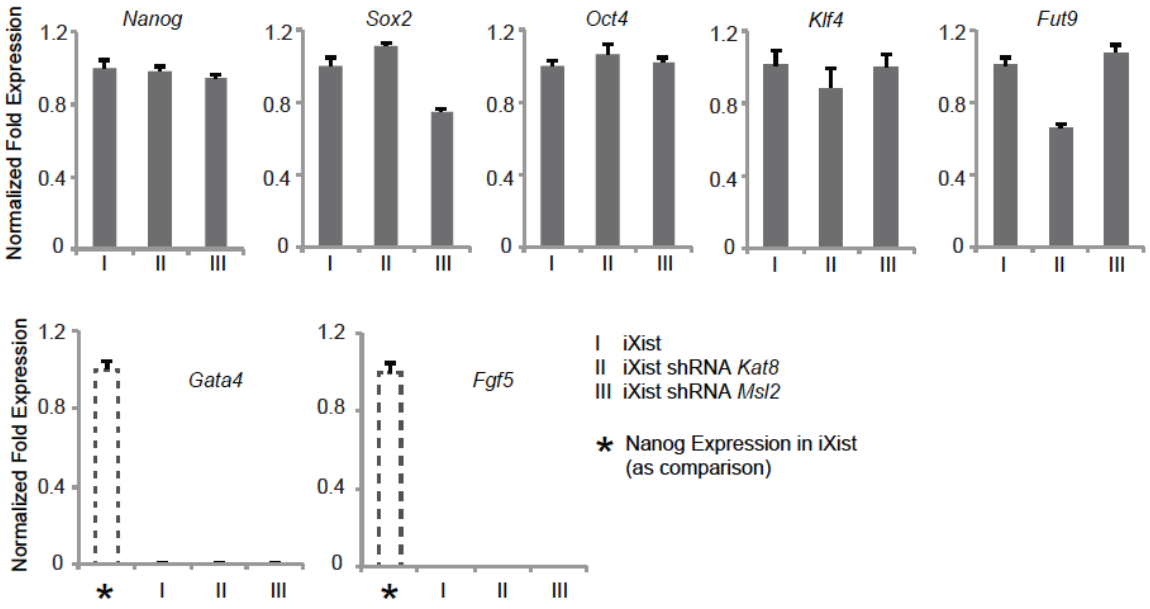

Figure S8: Expression profile of pluripotency-related genes in iXist and cells carrying shRNAs against *Kat8* and *Msl2* (Related to Figure 4).

Quantitative RT-PCR results are shown in relative fold expression. Normalization was performed using *Actb* and *Gapdh*. Error bars indicate SEM (n = 3). Cells were cultured as undifferentiated cells. *Nanog*, *Sox2*, *Oct4, Klf4* and *Fut9* are supposed to be expressed at high levels in undifferentiated cells. *Gata4* and *Fgf5* are not supposed to be expressed or expressed at very low levels in undifferentiated cells. To show the low expression levels of *Gata4* and *Fgf5*, *Nanog* expression level in iXist was included in the plots for direct comparison.

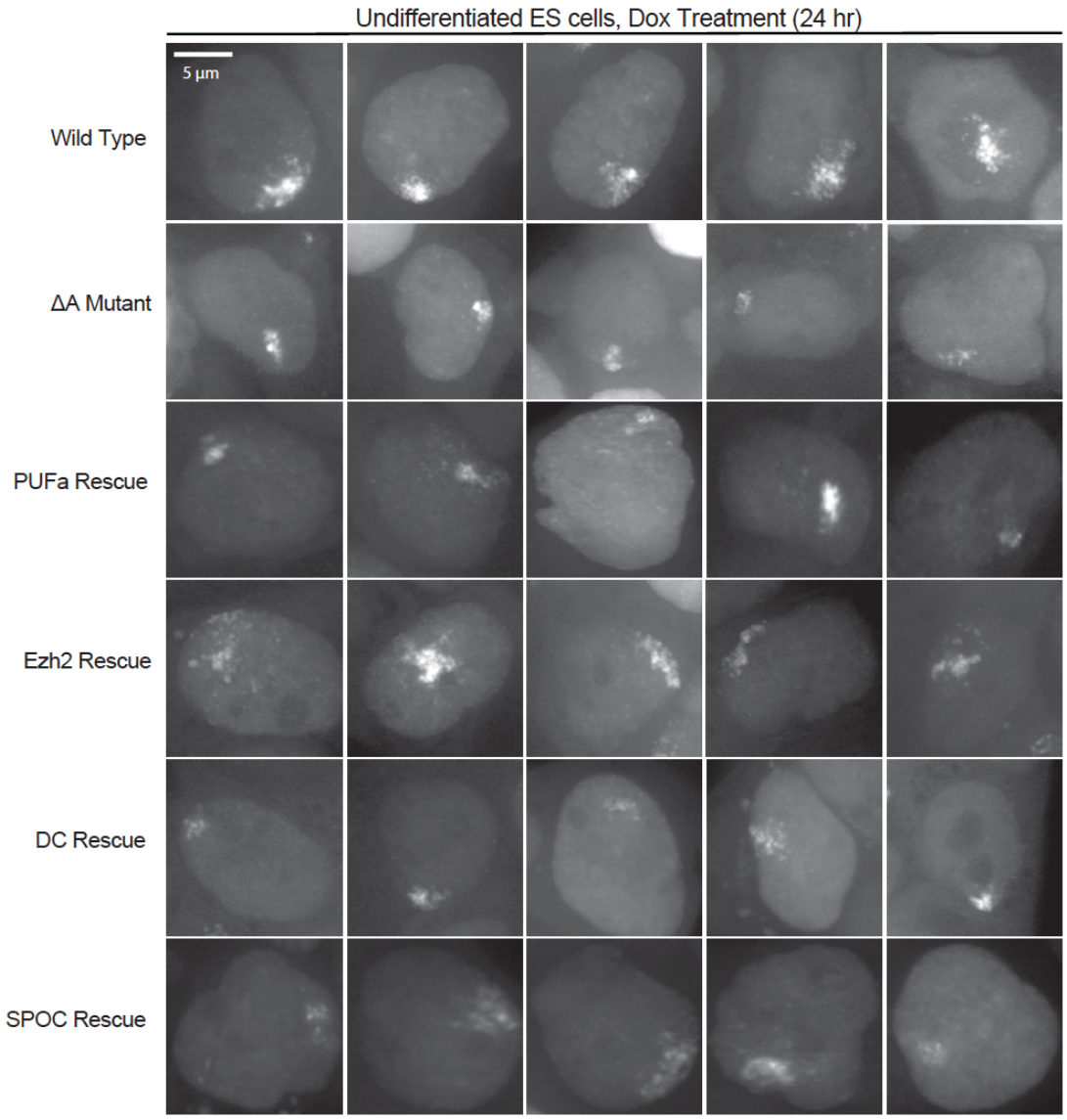

Figure S9: The Repeat A region of *Xist* is involved in the spreading of *Xist* RNA along the chromosome territory (Related to Figure 5). Cells were cultured as undifferentiated ES cells. Dox treatment was carried out for 24 hr. Representative images of *Xist* RNA signals in live cells are shown as maximum intensity z-projections.

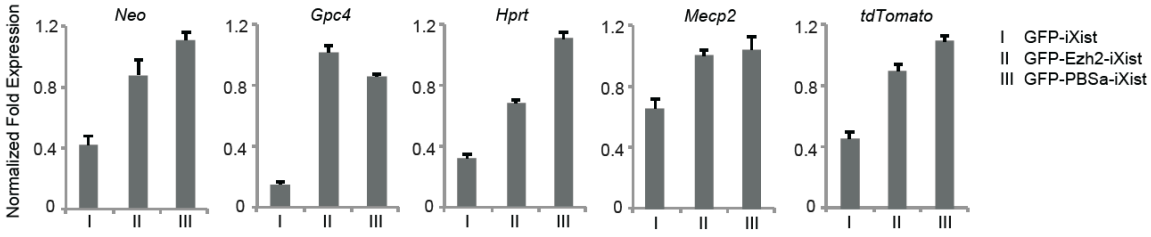

Figure S10: Quantitative RT-PCR results to show the effect of Ezh2-tethering on X-linked gene expression (Related to Figure 6). Cells were cultured as undifferentiated cells. Dox treatment was carried out for 24 hours. The results are shown in relative fold expression. Normalization was performed using *Actb*. Error bars indicate SEM (n = 3).

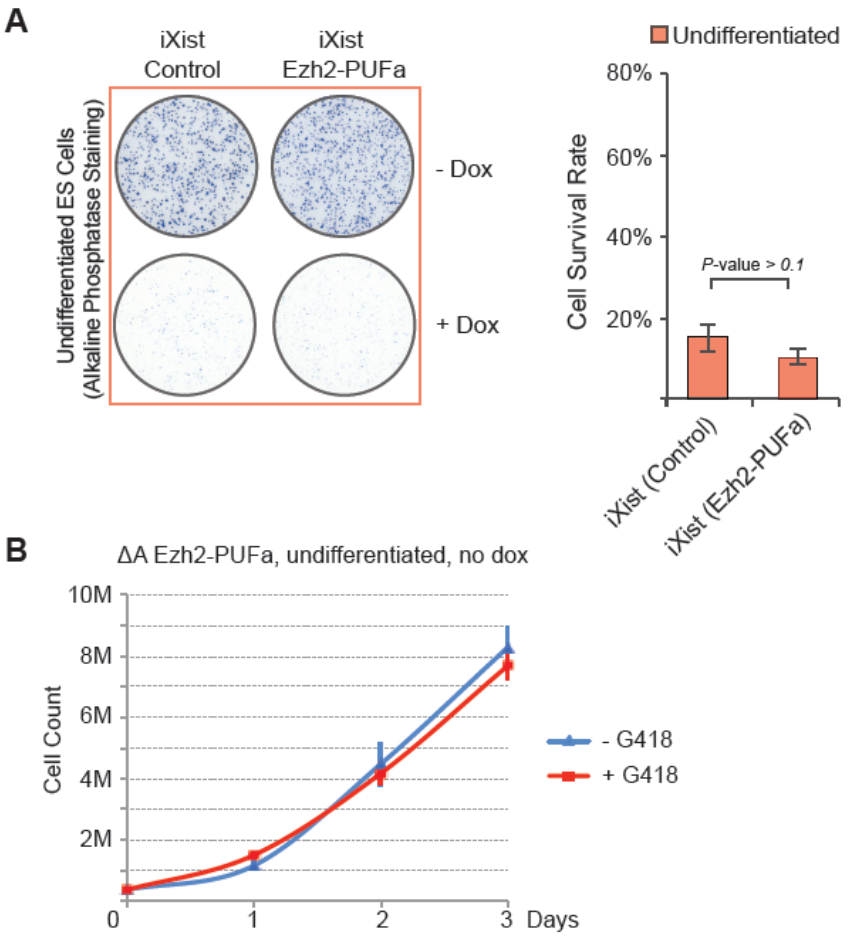

Figure S11: The side effects of Ezh2-PUFa overexpression without the induced *Xist* expression (Related to Figure 6). (A) Doxycycline-induced cell death assay was carried out for 6 days and alkaline phosphatase staining was performed. Data are shown as mean ± S.D. of biological triplicate. **(B)** The growth curves of Ezh2-PUFa overexpressing ΔA cells cultured with or without G418. Data are shown as mean ± S.D. of biological triplicate.

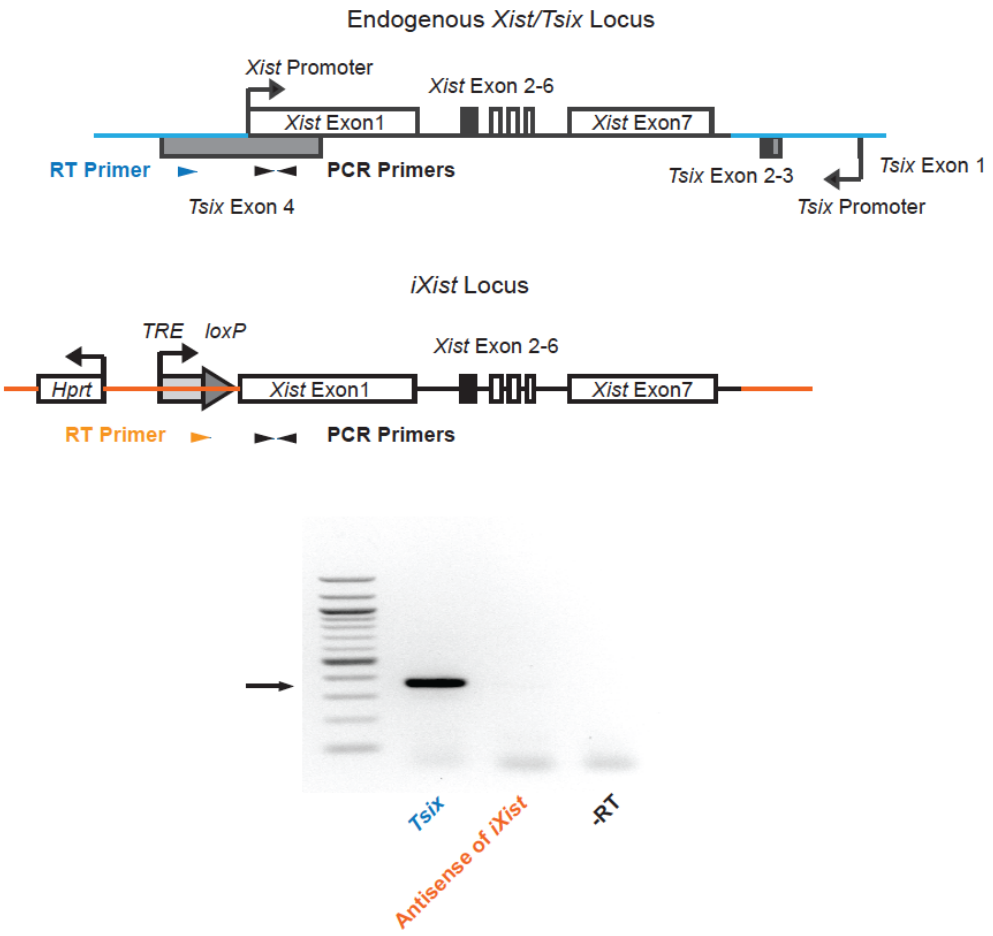

Figure S12: RT-PCR to detect the endogenous *Tsix* expression and the antisense transcription along the inducible *Xist* transgene (Related to Figure 4). Total RNA was isolated from undifferentiated iXist cells. Reverse transcription reactions were carried out using either a gene-specific primer for the endogenous *Tsix* (the blue arrowhead) or a gene-specific primer designed for the antisense transcription across the inducible *Xist* transgene (the orange arrowhead). cDNA samples were PCR amplified using a primer pair (the two black arrowheads) targeting the 5' region of *Xist* exon 1. The black arrow points to the PCR amplicon with the expected size.

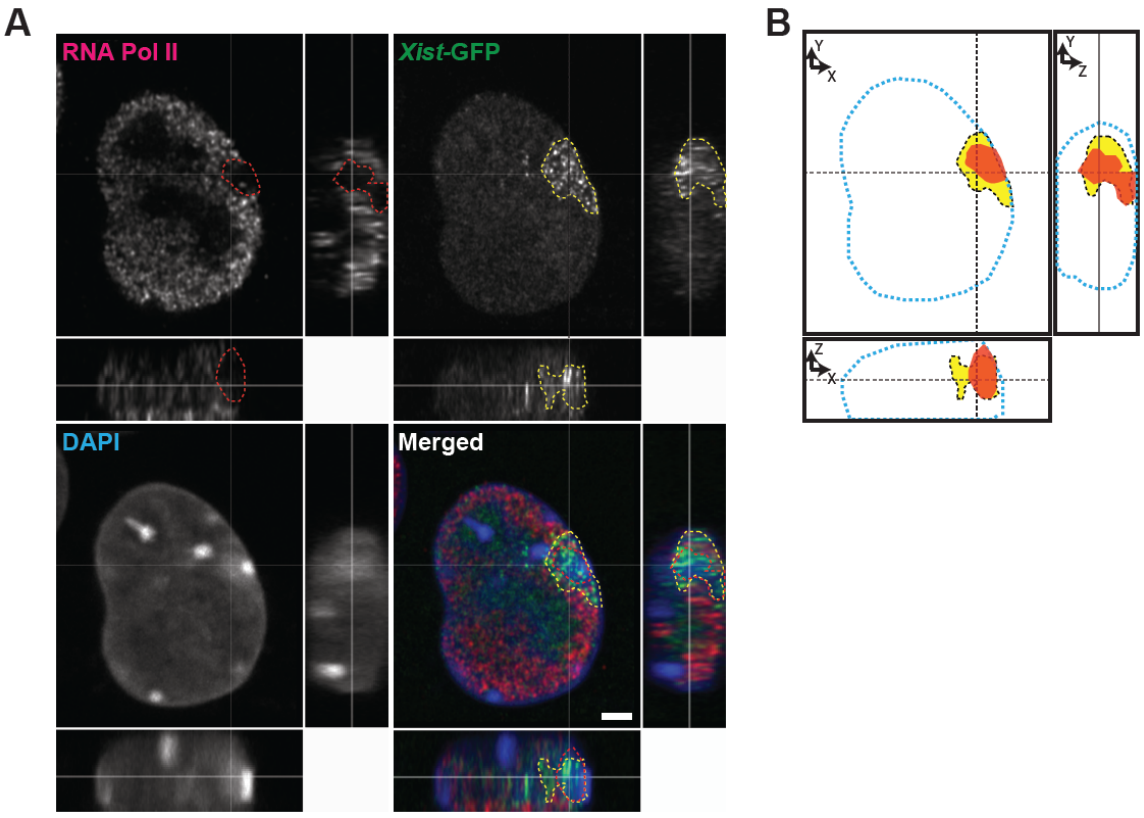

Figure S13: ImmunoRNA FISH of RNA polymerase II (Pol II) and *Xist* (Related to Figure 5). (A) Immunostain of Pol II on an undifferentiated GFP-iXist cell treated with dox for 24 hours. 3D localization of Pol II (Alexa 647), *Xist* (GFP) and DAPI were examined using Airyscan Super-resolution Confocal Microscope (Carl Zeiss) (X-Y: 36nm per pixel; Z: 140nm per pixel). Red dotted lines illustrate the silencing core territory of the *Xist* cloud without Pol II staining. Yellow dotted lines illustrate the main territory of the *Xist* cloud. Scale Bar: 2 μm. **(B)** Graphical illustration showing the Pol II staining pattern and the *Xist* cloud in 3D.

Transparent Methods

Cell lines and culture

If not explicitly stated otherwise, mouse ES cells were cultured in 2i medium with Lif (Ying et al., 2008). For in vitro differentiation, cells were cultured in differentiating medium containing 50 μg/ml L-ascorbic acid (Sigma). Doxycycline treatment of 1 μg/ml was used throughout the study. G418 (ThermoFisher)treatment was carried out at 400 μg/ml. Inhibitors for p300, L002(Sigma) and C646 (Sigma), were used at 10 μM and 25 μM respectively.

Alkaline phosphatase (AP) staining (Vector Laboratories) and Crystal Violet staining (Merck) were used to quantify undifferentiated ES cells and differentiating ES cells respectively. CellProfiler (Carpenter et al., 2006) and ImageJ (Schneider et al., 2012) were used to analyze AP staining data and Crystal Violet staining data respectively.

RNA FISH, immunostaining and immuno-RNA FISH

RNA FISH, immunostaining and immuno-RNA FISH were carried out as previously described (Zhang et al., 2007). Immunostaining for Nanog was performed using a rabbit polyclonal antibody against Nanog (Abcam; ab80892; 1:200) with a secondary antibody conjugated with Alexa-488 (ThermoFisher; A-11008; 1:1000). Immunostaining for Pol II was performed using a mouse monoclonal antibody against Pol II (Santa Cruz; sc-47701; 1:500) with a secondary antibody conjugated with Alexa-647 (ThermoFisher; A-21236; 1:500).

Immunostaining for H3K27me3 was performed using a mouse monoclonal antibody (Abcam; ab6002; 1:1000) with a secondary antibody conjugated with Alexa-647 (ThermoFisher; A-21236; 1:1000). Immunostaining for H2AK119ub was performed using a rabbit monoclonal antibody (Cell Signaling Technology; D27C4; 1:2000) with a secondary antibody conjugated with Alexa-647 (Abcam; ab150075; 1:1000). Immunostaining was followed by RNA FISH. The *Xist* RNA was detected with Sx9 probe, a P1 DNA construct containing a 40 kb genomic fragment covering the *Xist* gene. Nucleotide analogs used in probe labeling were Cy3-dUTP (Amersham, Cat# PA53022).

Quantitative RT-PCR

Total RNA was isolated by TRIzol (Life technologies). cDNA was synthesized using iScript reverse transcription kit (170-8840, Bio-Rad). The real-time PCR was carried out on the CFX Connect real-time PCR system (Bio-Rad) using the SsoAdvanced Universal SYBR Green Supermix (Bio-Rad). The following PCR primers were used: Actb (F:5'- ACTGCCGCATCCTCTTCCTC-3', R: 5'-CCGCTCGTTGCCAATAGTGA-3'); Gapdh (F:5'-CCAATGTGTCCGTCGTGGAT-3', R: 5'-TGCCTGCTTCACCACCTTCT-3'); Nanog (F:5'-TCGAATTCTGGGAACGCCTC-3', R: 5'-GTCTTCAGAGGAAGGGCGAG-3'); Sox2 (F:5'-TTCGAGGAAAGGGTTCTTGCTG-3', R: 5'-TCCTTCCTTGTTTGTAACGGTCCT-3'); Oct4 (F:5'-TGTTCCCGTCACTGCTCTGG-3', R: 5'-TTGCCTTGGCTCACAGCATC-3'); Klf4

(F:5'-GTGCCCCGACTAACCGTTG-3', R: 5'-GTCGTTGAACTCCTCGGTCT-3'); Fut9 (F:5'-CAGTCCAATGGAGTCTGCAA-3', R: 5'-CCATACCCAAACCAGAATGG-3'); Gata4 (F:5'-CCTGGAAGACACCCCAATCTC-3', R: 5'-GGTAGTGTCCCGTCCCATC-3'); Fgf5 (F:5'-CCTTGCGACCCAGGAGCTTA-3', R: 5'-CCGTCTGTGGTTTCTGTTGAGG-3'); Kat8 (F:5'-AACCAGAAGTCACCGTGGAG-3', R: 5'-TCCTGGTCATTCACTCGAGAC-3'); Msl2 (F:5'-CCCGGTGACTCTCTTTTGCT-3', R: 5'-GCTTCCAAGTTTGGCTGCAA-3')); Mecp2 (F:5'-CAGGGAGGAAAAGTCAGAAGACC-3', R: 5'AATGGTGGGCTGAAGGTTGTA-3'); Hprt (F:5'-GATTAGCGATGATGAACCAGGTT-3', R: 5'-CCTCCCATCTCCTTCATGACA-3'); Gpc4 (F:5'-GGCAGCTGGCACTAGTTTG-3', R: 5'-AACGGTGCTTGGGAGAGAG-3'); Neomycin (F:5'-GGCTATTCGGCTATGACTGGGC-3', R: 5'-GCAGTTCATTCAGGGCACCG-3'); tdTomato (F:5'-CCGACATCCCCGATTACAAGAAGC-3', R: 5'-TTGTAGATCAGCGTGCCGTC-3'); *Xist* (E1_F: 5'-CGGCCTCTAGTTTGTCCATT-3', E1_R: 5'-GATGGCATGATGGAATTGAG-3').

Plasmid Constructs

PBS and PUF plasmids were obtained as gifts from Dr. Wang Haoyi. *galK*-mediated recombineering system was used to generate all the DNA constructs of inducible *Xist* transgenes (Warming et al., 2005).

A human *SPEN* cDNA (~11kb) clone was purchased from OriGene (RC213922). A frame shift mutation (3351_3352insA) within the coding region of *SPEN* was found in the original cDNA clone. The coding region of the SPOC domain is intact and was PCR amplified. cDNA of Ezh2 and Ythdc1 were generated using SuperScript III reverse transcriptase kit (ThermoFisher) followed by PCR amplification using Herculase II Fusion Enzyme (Agilent Technologies). The sequences of the cloned cDNA fragments of SPOC, Ezh2 and Ythdc1 were confirmed by Sanger sequencing (data not shown). The following PCR primers were used: Ezh2 (F:5'-ATGGGCCAGACTGGGAAGAAATC-3', R:5'-CATTTCTCGTTCGATGCCCACATAC-3'); Ythdc1 (F:5'-ATGGCGGCCGACAGC-3', R:5'- AACGACCTCTCTCCCCTCGG-3'); SPOC (F:5'-ATGCCTCAAGTGTCCCAGGAG-3', R:5'-AATGACAATCATGAGGTGGGGAGAG-3'). Plasmid constructs for fusion proteins, PUF-EGFP and PUF-effector, were established using Gibson Assembly (NEB).

An shRNA system (OligoEngine, pSUPER RNAi System) was used. The following shRNA sequences were designed against *Msl1* (5'-GTACCTTTCCACCACAGAAAT-3'), *Msl2* (5'-CCCAGTCTCTTAGCCATAATG-3'), *Msl2-2*(5'- CTGATCCTCAAGCTAGCTTAT-3'), Msl3 (5'-GCTGCGTTCAAGAAAGGAAAT-3'), *Kat7* (5'-CCTCGAACTCCAACCGGAAAT-3') and *Kat8* (5'-GTGATCCAGTCTCGAGTGA-3'), *Kat8-2*(5'-GCGAAAGCATGATGAGATCAA-3').

Microscopy

Wide-field fluorescent microscopy work was carried out on an Eclipse Ti microscope (Nikon) with a digital camera (Clara Series model C01, Andor). Airyscan microscopy was carried out on a Zeiss LSM 710 inverted confocal microscope with Airyscan detector and an oil immersion alpha Plan-Apochromat 100x/1.4 Oil M27 objective lens.

Live-cell imaging was carried out on a CorrSight spinning disk confocal system (FEI Company) equipped with an Orca R2 CCD camera (Hamamatsu). 1 day before imaging, 800K feeder-free ES cells were seeded on fibronectin-coated glass-bottom dishes (MatTec Corp). Prior to live-cell imaging, cells were washed with 1x PBS and replaced with imaging medium composing complete medium with DMEM substituted with FluoroBrite DMEM (ThermoFisher). For sunrise experiments, 1 μg/ml of doxycycline was supplemented to the imaging medium to induce *Xist* expression. For sunset experiments, *Xist* was induced by 1 μg/ ml of doxycycline for at least 16 hr. The cells were washed a few times using 1x PBS. The culture medium was then switched to the imaging medium free of doxycycline. For live-cell time-lapse video recording, cells were placed into the microscope cell culture chamber heated to 37 °C at least 1 hr before imaging. Imaging was carried out in a closed chamber maintained at 37 °C with 5% CO2 and 90% humidity. DNA dyes, such as Hoechst, was avoided due to its toxicity in long-term live-cell imaging. A 488-nm laser line (iChrome MLE-LFA) was set at 100% laser power. Images were acquired using a PlanApo 63x/ 1.4

N.A. oil-immersion objective (Zeiss) (heated to 37 °C) with standard filter sets. The exposure time was set at 200 ms. All live-cell time-lapse video recording, unless explicitly stated otherwise, was carried out in a 2-hr time span with a 2-min time interval. For each time point, a 10-μm thick Z-stack with a 1-μm interval was collected. Autofocus system (Focus Clamp) was used to minimize out-of-focus throughout the recordings. Time-lapse imaging was started 2 hr after the addition of doxycycline for undifferentiated cells and 1 hr after the addition of doxycycline for differentiating cells. Other than time-lapse video recording, the snap-shot images of *Xist* signals in live cells were captured with an 800-ms exposure time at 100% laser power in 10-μm Z-stacks at 1-μm intervals. Maximum intensity Z-projection was used to represent each Z-stack. All acquired images were processed and analyzed using ImageJ (Schneider et al., 2012). Drift correction was applied to all time-lapse recordings.

Statistical analyses

All data were analyzed by one-tailed Student's *t*-test for equal variances and were conducted in Excel. A *P*-value that is less than 0.05 is considered statistically significant. Statistical tests used for all experiments were described in detail in the relevant figure legends of the Results and Supplemental Information.

Supplemental References

CARPENTER, A. E., JONES, T. R., LAMPRECHT, M. R., CLARKE, C., KANG, I. H., FRIMAN, O., GUERTIN, D. A., CHANG, J. H., LINDQUIST, R. A., MOFFAT, J., GOLLAND, P. & SABATINI, D. M. 2006. CellProfiler: image analysis software for identifying and quantifying cell phenotypes. *Genome Biol,* 7**,** R100.

SCHNEIDER, C. A., RASBAND, W. S. & ELICEIRI, K. W. 2012. NIH Image to ImageJ: 25 years of image analysis. *Nat Methods,* 9**,** 671-5.

WARMING, S., COSTANTINO, N., COURT, D. L., JENKINS, N. A. & COPELAND, N. G. 2005. Simple and highly efficient BAC recombineering using galK selection. *Nucleic Acids Res,* 33**,** e36.

YING, Q. L., WRAY, J., NICHOLS, J., BATLLE-MORERA, L., DOBLE, B., WOODGETT, J., COHEN, P. & SMITH, A. 2008. The ground state of embryonic stem cell self-renewal. *Nature,* 453**,** 519-23.

ZHANG, L. F., HUYNH, K. D. & LEE, J. T. 2007. Perinucleolar targeting of the inactive X during S phase: evidence for a role in the maintenance of silencing. *Cell,* 129**,** 693-706.